Biogeosciences, 23, 4691–4710, 2026
https://doi.org/10.5194/bg-23-4691-2026
© Author(s) 2026. This work is distributed under
the Creative Commons Attribution 4.0 License.

Biogeosciences Open Access EGU

Ocean alkalinity enhancement reduces silica ballasting during export due to amplified dissolution

Philipp Suessle[1,3], Kai Georg Schulz[2], Joana Barcelos e Ramos[1], Nico Manuel Sievers[3], Julieta Schneider[2,3], Juliane Katharina Tammen[3], Leila Kittu[3], Laura Marín-Samper[4], Maarten Boersma[5], and Ulf Riebesell[3]

[1]Group of Climate, Meteorology and Global Change, Institute of Agricultural and Environmental Research and Technology, University of the Azores, 9700-042 Angra do Heroísmo, Portugal
[2]Faculty of Science and Engineering, Southern Cross University, Lismore, NSW, Australia
[3]GEOMAR Helmholtz Centre for Ocean Research Kiel, Wischhofstrasse 1–3, 24148 Kiel, Germany
[4]Instituto de Oceanografía y Cambio Global, Universidad de Las Palmas de Gran Canaria, 35017 Telde, Spain
[5]Alfred-Wegener-Institut; Helmholtz-Zentrum für Polar- und Meeresforschung, Wadden Sea Station Sylt, Hafenstrasse 43, 25992 List, Germany and FB2 University of Bremen, Bremen, Germany

Correspondence: Philipp Suessle (philippsuessle@gmx.de)

Received: 9 March 2026 – Discussion started: 12 March 2026
Revised: 5 June 2026 – Accepted: 26 June 2026 – Published: 8 July 2026

Abstract. Ocean alkalinity enhancement (OAE) is a carbon dioxide removal (CDR) technology proposed to store carbon dioxide (CO_2) in the ocean on human-relevant time scales. However, depending on OAE intensity, resulting shifts in seawater carbonate chemistry speciation could alter community-driven biomass build-up, particulate stoichiometry, and transformation during particle export. Using mesocosms in the eutrophic North Sea (Helgoland, Germany), we established six alkalinity levels under two dilution scenarios (localized vs. uniform OAE additions) for 39 d. Total alkalinity (TA) was increased to $\Delta TA_{max} = 1250\,\mu mol\,kg^{-1}$ ($250\,\mu mol\,TA\,kg^{-1}$ increments) using NaOH with $CaCl_2$ to simulate cation release during calcium-based mineral dissolution, causing strong carbonate chemistry perturbations (e.g., $pH_{max} > 9.25$). To compare community-mediated carbon export across equivalent bloom phases, measurements were assessed within mesocosm-specific bloom and export events rather than on fixed sampling days, thereby accounting for OAE-induced shifts in spring bloom timing. During blooms, average phytoplankton biomass (as the concentrations of chlorophyll *a* and particulate organic carbon in the water column, POC_{WC}) remained unchanged under unequilibrated OAE. In contrast, silica ballasting ratios declined with increasing pH_T: suspended biogenic silica to particulate organic carbon ratios ($BSi_{WC} : POC_{WC}$, where WC = water column) decreased by up to 50 %, while exported $BSi_{Sed} : POC_{Sed}$ (where Sed = sediment) decreased by 60 %, indicating intensification during sinking. The stronger decline in sinking compared to suspended BSi : POC is consistent with pH-enhanced BSi dissolution during export. Porosity of sinking particles increased with pH_T and co-varied with $BSi_{Sed} : POC_{Sed}$, suggesting particle-quality traits can modulate dissolution during transit. Organic matter remineralization metrics showed no response to alkalinity addition, and particle sinking velocities did not scale with suspended or sinking silica ballasting ratios. Across dilution scenarios, unequilibrated OAE may reduce silica ballasting, potentially shoaling carbon remineralization, shortening sequestration timescales, and weakening net CO_2 removal, while effects of dissolved silica regeneration on diatom productivity remain unresolved. Quantifying how pH-driven BSi dissolution interacts with bloom and export dynamics will be critical for evaluating OAE efficacy and ecological safety.

1 Introduction

Ocean alkalinity enhancement (OAE) is a carbon dioxide removal (CDR) strategy which may help restrict global warming to 2 °C (Renforth and Henderson, 2017; Rogelj et al., 2018). By delivering alkaline material to the ocean (Gattuso et al., 2018; Renforth and Henderson, 2017), OAE shifts sea-

water carbonate speciation towards carbonate (CO_3^{2-}) and bicarbonate (HCO_3^-), thereby lowering seawater carbon dioxide fugacity (fCO_2) and promoting further atmospheric uptake (Zeebe and Wolf-Gladrow, 2007). Model-based estimates suggest that, if deployed sufficiently widely, the process is capable of sequestering CO_2 on gigaton scales (3–30 Gt yr^{-1}; Feng et al., 2017; Köhler et al., 2010; Renforth and Henderson, 2017) and may potentially mitigate effects of ocean acidification (Doney et al., 2009; Gattuso et al., 2015). Various OAE strategies have been proposed, with several already in practice, ranging from alkaline solution injection and mineral additions to electrochemical approaches (Eisaman et al., 2023). Yet their impacts on marine communities and the carbon sequestration they drive remain poorly understood, highlighting the need to evaluate OAE's overall CO_2 removal potential (Bach et al., 2019a; Gattuso et al., 2021; Suessle et al., 2025).

Marine organisms do not perceive alkalinity enhancement directly (Bach et al., 2019a), instead, the transient carbonate-chemistry shifts prior to atmospheric re-equilibration can influence plankton growth, community composition, and microbial processing (Antoni et al., 2025; De Castro et al., 2025; Ferderer et al., 2022; Marín-Samper et al., 2024b; Oberlander et al., 2025). Such responses can modify the efficiency of the biological pump (Boyd and Newton, 1999; Guidi et al., 2009), a process that sequesters atmospheric CO_2 (5–12 Gt yr^{-1}; Boyd et al., 2019; Siegel et al., 2014) by gravitational settling of biogenic material from the surface to the deep ocean (Sarmiento, 2006). In many productive systems, diatom blooms dominate this export flux production, and diatom-derived particulate biogenic silica (BSi) provides ballast for aggregates that increases sinking velocities and shifts particulate organic carbon (POC) remineralization to greater depths (Armstrong et al., 2001; Honjo et al., 2008). Under OAE, reduced CO_2 availability could delay or dampen diatom blooms or increase reliance on carbon concentrating mechanisms (CCMs), with the potential to shift competitive balances among taxa and alter diatom community composition and associated size structure (Bach and Taucher, 2019; Hansen, 2002; Pierella Karlusich et al., 2021; Raven, 1993; Riebesell et al., 1993; Sommer et al., 2015). These shifts could in turn affect export pathways, as cell and particle size influence zooplankton grazing and thus the repackaging of organic matter into fast-sinking fecal pellets (Le Moigne et al., 2016; Stukel et al., 2011). In addition, BSi dissolution increases with pH and follows well-characterized reaction kinetics, such that OAE-driven pH perturbations are expected to reduce silica preservation during sinking and weaken ballasting, with converging support from laboratory and globally relevant field observations (Socratis et al., 2008; Taucher et al., 2022; Van Cappellen et al., 2002). However, most OAE studies primarily constrain production-side responses (e.g., diatom silicification or growth; De Castro et al., 2025; Ferderer et al., 2025; Iglesias-Rodríguez et al., 2023; Oberlander et al., 2025) but rarely resolve transformations in diatom biomass along the sinking pathway. This is a key gap as ocean-acidification studies show that production-side responses of diatoms and silica formation can vary in sign and magnitude across contexts (Dutkiewicz et al., 2015; Gao and Campbell, 2014), whereas export-phase BSi dissolution provides clear directionality under pH perturbations. OAE-induced pH increases could therefore weaken silica ballasting with depth, even when biomass build-up or community composition changes are only modest.

Where and how OAE is deployed will largely determine its ecological impacts and safe operating ranges (Dupont and Metian, 2023). To date, experiments in oligotrophic or subtropical settings suggest that dissolved alkalinity additions (e.g., NaOH-based) have limited effects on community composition, microbial rates, and associated export, consistent with low nutrient availability and weak bloom/export signals (Marín-Samper et al., 2024a; Sánchez et al., 2024; Subhas et al., 2022; Suessle et al., 2025), with OAE feedstock-specific effects, such as trace-metal release, remaining a relevant caveat (Guo et al., 2025). In contrast, coastal regions are often considered more attractive for deployment due to logistical proximity to resources (Bach et al., 2019a; He and Tyka, 2023), but exhibit strong nutrient and temperature variability, recurrent blooms, and rapid community succession (Cloern, 1996; Kauppi et al., 2017). Although coastal regions only occupy a small fraction of the ocean surface, they are typically diatom-dominated (Abrantes et al., 2016; Malviya et al., 2016) and contribute disproportionately to global biological carbon sequestration (Borges et al., 2005; Mathis et al., 2024; Stukel et al., 2023). Moreover, coastal OAE is likely to occur via localized inputs (Eisaman et al., 2023), creating transient hotspots in alkalinity, pH, and fCO_2 with magnitude and persistence depending on local dilution and mixing (Anderson et al., 2025; Bach et al., 2019a), influencing the severity of ecological and export responses. Elevated alkalinity may also trigger unintended calcium carbonate precipitation when local carbonate saturation states become sufficiently high, particularly under concentrated or poorly diluted OAE additions (Hartmann et al., 2023; Hashim et al., 2025; Moras et al., 2022; Schulz et al., 2023). Such precipitation consumes alkalinity and can reduce the effective CO_2 uptake potential of OAE (Bach et al., 2019a; Hashim et al., 2025), while simultaneously altering carbon export pathways by forming ballast material associated with sinking particles (Suessle et al., 2025). In that sense, constraining OAE effects on biomass production and export efficiency in such productive coastal systems across a wide pH range is essential before large scale deployment.

Here, we assessed the sensitivity of diatom-mediated export production and measured silica ballasting ratios (BSi : POC) of a plankton community from the North Sea (Helgoland, Germany) to CO_2-unequilibrated, carbonate-based OAE. Enclosing natural communities in mesocosms (initial volume $\sim 5.9\,m^3$) for 39 d, six alkalinity levels ($\Delta TA_{max} = 1250\,\mu mol\,kg^{-1}$) were applied using NaOH and

$CaCl_2$ under two dilution regimes (Fig. 1). The experiment was originally designed to contrast idealized scenarios of point-source and dispersed OAE additions (e.g., ship-based, see Caserini et al., 2021), simulating varying degrees of dilution associated with discharge method and oceanographic state. Here, we prioritized analysis along the shared pH_T gradient to isolate alkalinity-driven controls on bloom development and export (while retaining dilution-specific results for transparency). This study addresses a key gap in current OAE research by resolving how strong carbonate-chemistry perturbations affect diatom-mediated silica ballasting ratios across both suspended and sinking particulate pools in a productive coastal system. By separating water-column from exported material across a wide pH_T gradient, our design provides mechanistic constraints on whether OAE alters biogenic silica preservation during export and thereby the efficiency of the biological pump.

2 Methods

2.1 Experimental setup and alkalization

On 12 March 2023, twelve in situ mesocosms were deployed in the south harbour of Helgoland (54° 10‘36.9“ N, 7° 53‘36.0“ E; North Sea, Germany, see Alfred-Wegener-Institut Helmholtz-Zentrum für Polar- und Meeresforschung, 2023) to investigate the effect of OAE on biogeochemical responses of a temperate eutrophic community from the North Sea. Each mesocosm consisted of a transparent cylindrical polyurethane bag ($Ø = 2$ m), which ended in a 1.6 m conical sediment trap, with an overall length of 3.5 m. It was suspended in a polyethylene floating frame, allowing for the observation of pelagic communities under natural temperature and light conditions. The mesocosms were filled with seawater originating from the Helgoland Roads observatory site (Wiltshire et al., 2010; water depth at site $\sim$6–8 m). Using a peristaltic pump, water from 2–3 m depth (minimizing benthic influence) was screened (< 3 mm) and transferred into an intermediate reservoir. From there, all mesocosms were filled simultaneously with $\sim 5.9\,m^3$. Pumping speed averaged $\sim 14\,m^3\,h^{-1}$ to minimize biological stress, resulting in a $\sim$12 h filling-process (for technical details see Bach et al., 2019b). Filling took place on 13 March, marking day zero of the experiment. The days preceding the OAE manipulation (day 4) were used for baseline characterization of various water column parameters, while sediment-trap samples from these initial days were discarded due to filling-related particle disturbance. Additionally, CTD profiles (CTD60M, Sea & Sun Technology GmbH, Germany) measured temperature, salinity, pH, chlorophyll *a*, dissolved oxygen, and photosynthetically active radiation before OAE manipulation to ensure homogeneity across mesocosms and alignment with conditions at the Helgoland Roads site (Wiltshire et al., 2010). We note that enclosure and the four-day pre-manipulation confinement period may have influenced community development relative to ambient field conditions. However, because all mesocosms experienced the same filling and confinement history prior to OAE manipulation, such effects are unlikely to confound the post-manipulation treatment comparisons presented here. The OAE manipulation was simulated using a CO_2-unequilibrated approach, meaning that dissolved inorganic carbon (DIC) was not raised alongside TA, deliberately resulting in strong (yet transient) perturbations of seawater carbonate chemistry (e.g. pH_T, $\Omega_{Ca\,/\,Ar}$) until re-equilibration with the atmosphere (Bach et al., 2019a; Renforth and Henderson, 2017). Accordingly, this strategy was chosen since it reflects a more realistic pathway for large-scale and economically feasible OAE implementation than CO_2 pre-equilibration of solutions prior to alkalinity release (He and Tyka, 2023). While the study-design encompassed varying dilution scenarios, to differentiate impacts of point-based versus more uniform alkalinity perturbations (Eisaman et al., 2023), here we will prioritize analysis of response signals over the common alkalinity/pH gradient. Informing about environmental safety of varying application modes remains relevant, but equally important is the assessment of the net CO_2 sequestration outcome of OAE when factoring in potential changes to the biological carbon pump. This focus reflects both the broader relevance of alkalinity-driven bloom and export responses for evaluating net CO_2 sequestration outcomes, and the inherent limitations of sediment-trap-based export metrics for resolving dilution-specific signals as integrated sinking material cannot be attributed to a specific depth layer of origin. For coherence with other publications coming from this experiment, the full treatment design is described below and the corresponding colour coding is retained in all figures.

The carbonate chemistry manipulation was realized 4 d after filling and aimed to simulate calcium-based OAE using NaOH and stoichiometrically proportionated $CaCl_2$ solutions to mimic cation release during mineral dissolution. Therefore, the mesocosms were strategically assigned to two sets of six: one set received alkalinity throughout the enclosed water column (immediate dilution), representing an idealized rapid-dilution of alkalized waters and conceptually related to well-mixed upper-mixed-layer application modes, such as ship-wake release (Caserini et al., 2021), while the other set was initially alkalized only in the top layer (delayed dilution) and mixed after 2 d. For this, 17 L of $CaCl_2$ solution (in pre-filtered freshwater) were applied evenly across the perimeter of the mesocosm using a custom-built device (see Riebesell et al., 2013 for technical details), either over the entire depth (immediate) or only within the top 80 cm (delayed). To ensure full treatment delivery, an additional 17 L of freshwater was flushed into each mesocosm, applied either across the full depth or surface-only, further solidifying stratification in the delayed treatment through density differences ($\Delta PSU \approx 0.5$). Concentrations of $CaCl_2$ solutions corresponded to half of the respective target alkalinity additions.

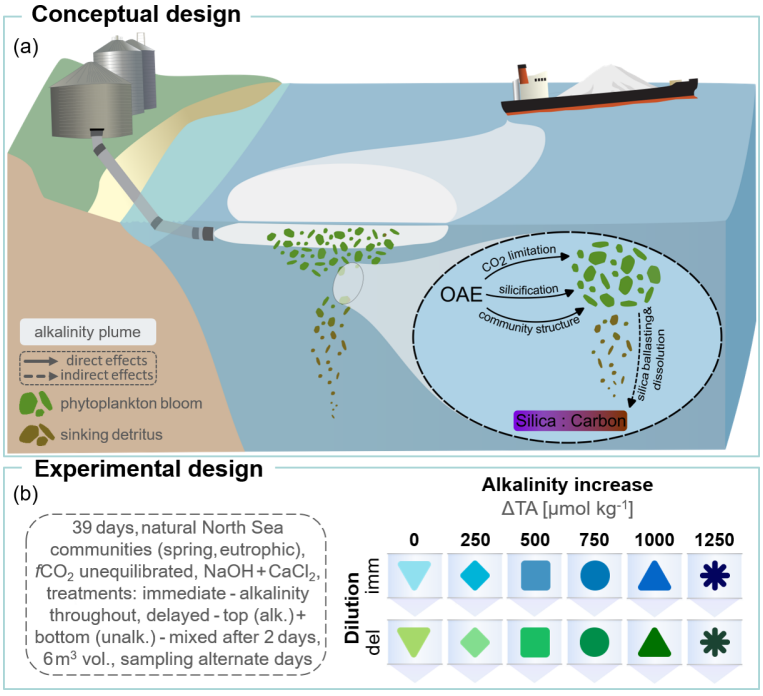

Figure 1. Conceptual and experimental framework of our mesocosm study on CO_2 unequilibrated OAE. **(a)** Potential application scenarios and pathways by which OAE may change phytoplankton biomass, stoichiometry and subsequent export. **(b)** Setting and manipulation using 12 mesocosms subjected to two idealized dilution scenarios. Delayed dilution (del) represents a localized, surface-intensified perturbation, as may occur near point-source additions, whereas immediate dilution (imm) represents a more distributed upper-mixed-layer perturbation, conceptually relevant to well mixed conditions following alkalinity release. Levels in ΔTA given relative to background alkalinity of 2340 µmol kg^{-1}. Graphics adapted from Integration and Application Network, University of Maryland Center for Environmental Science https://ian.umces.edu/symbols/, last access: 21 October 2025).

This calculation assumes $Ca(OH)_2$-based OAE, where dissolution of one mole of $Ca(OH)_2$ releases one mole of Ca^{2+} and two equivalents of alkalinity. To raise alkalinity, NaOH solutions (in pre-filtered freshwater) were then added using the same device, either throughout the full water column (immediate) or confined to the surface (delayed). In the delayed treatments, upper-layer alkalinity concentrations were intended to be doubled relative to the immediate treatments so that, the intended target alkalinity levels were reached only after mixing of the water column two days later. Alkalinity concentrations (post-mixing) were applied in increments of 250 µmol TA kg^{-1}, reaching $\Delta TA = 1250$ µmol kg^{-1} relative to a background alkalinity of 2330 µmol kg^{-1}. To achieve mixing of the delayed dilution treatments and avoid procedural bias across treatments, all mesocosms were homogenized by bubbling pressurized air through the sediment trap, 48 h after manipulation. The order of $CaCl_2$ application was randomized, while NaOH application proceeded from lowest to highest treatment to avoid carryover effects, alternating between equivalent levels of delayed and immediate dilution scenarios. Control mesocosms were treated similarly throughout the manipulation, but with freshwater only. Mooring positions along the pier were randomized in order to not have an alkalinity gradient along a natural one such as light availability. A schematic overview of the treatment setup and manipulation timeline is provided in Fig. S1 in the Supplement. For details on changes in carbonate chemistry parameters see Fig. S2.

We note that CO_2 equilibration during our experiment was minimal (Fig. S2) yet realistic, considering that CO_2 re-equilibration with the atmosphere after alkalinity enhancement will typically take months to years under natural oceanographic conditions as well (He and Tyka, 2023; Jones et al., 2014) and was similar to other OAE mesocosm studies (Schneider et al., 2026). Accordingly, TA targets were intentionally high to maximize detectability of biological responses across a wide pH range and the use of NaOH allowed for complete and rapid mixing, enabling controlled and precise TA additions (Iglesias-Rodríguez et al., 2023).

2.2 Sampling procedure and maintenance

Sampling was initiated on day one using a polypropylene tube integrating the upper 2 m of the water column with a volume of 4.5 L. Upon treatment additions, but prior to mixing (days five and six), samples in the delayed dilution mesocosms were collected separately from the top and bottom layers using 5 L Niskin bottles (Hydro-Bios, Kiel, Germany).

Bulk water samples for the immediate dilution treatments continued to be taken with a polypropylene tube sampler. Post-mixing, all mesocosms were sampled every 2 d between 09:00 and 12:00 am (UTC+1) using the same integrating polypropylene tube sampler. A CTD60M (Sea & Sun Technology GmbH, Germany) was cast in the beginning of every sampling for abiotic parameters such as temperature, salinity, pH, Chl *a*, dissolved oxygen (O_2) and photosynthetically active radiation. Then, per sampling occasion, 15–30 L of water were sampled (4–7 tubes), distributed into several containers dedicated to different analyses, and generally kept dark and at in situ temperature until returned to the laboratory. Particulate material collected in the sediment traps (PM_{Sed}) was retrieved through a pre-fixed silicone hose with a manual vacuum pump, maintaining pressures below 0.3 bar. The material was transferred into 5 L glass bottles (Schott Scandinavia A/S, Kgs, Denmark) and stored in the dark until processed in the laboratory (see Boxhammer et al., 2016 for technical details). Whenever subsamples were required, the sediment was gently re-suspended by rotating the bottles, ensuring a homogeneous mixture before withdrawal for further analyses. To limit shading and nutrient consumption caused by organism growth, the inner walls of the mesocosms were cleaned with brushes every 6 d. To further counteract shading, divers cleaned the outer walls with brushes on three occasions during the experiment.

2.3 Parameters

2.3.1 Sediment trap particulate matter fluxes and stoichiometry

PM_{Sed} samples were processed for determination of total particulate carbon and nitrogen (TPC / N_{Sed}), as well as particulate organic carbon, total particulate phosphorus (POC_{Sed}, TPP_{Sed}), and biogenic silica (BSi_{Sed}). Particles were separated from seawater by enhancing coagulation and flocculation through the addition of 3 mol L^{-1} ferric chloride ($FeCl_3$) to the 5 L sediment bottles, followed by 3 mol L^{-1} NaOH to counteract pH reduction, thereby promoting efficient particle recovery (Boxhammer et al., 2016). After 1 h of settling, the supernatant was carefully removed and the concentrated suspension was centrifuged for 10 min at 5200 g (6–16 KS, Sigma Laborzentrifugen GmbH, Germany). A second centrifugation step (10 min at 5000 g, 3K12 centrifuge, Sigma) produced compact sediment pellets. These pellets were stored at −20 °C and later shipped to Kiel for laboratory analysis. At GEOMAR, the frozen material was freeze-dried to eliminate residual moisture and subsequently homogenized into a fine powder using a cell mill (Edmund Bühler GmbH, Germany). The sediment powder was preserved in glass or plastic vials under cool and dark conditions. For analysis, the powder was transferred into silver (POC) or tin capsules (TPC / N): samples destined for POC_{Sed} determination were acidified with 1 mol L^{-1} HCl and dried overnight at 50 °C, while those for TPC / N_{Sed} analysis remained untreated. Duplicate measurements were conducted with a CN analyzer (Euro EA-CN, HEKAtech GmbH, Germany) following the protocol of Sharp (1974). Accuracy was monitored by measuring acetanilide standards of known C and N content between samples. Precision was estimated from the average standard deviation between duplicate measurements over the course of the experiment and amounted to ± 0.03 µmol TPC L^{-1} d^{-1}, ± 0.01 µmol TPN L^{-1} d^{-1}, and ± 0.04 µmol POC L^{-1} d^{-1}, respectively. Concentrations of particulate inorganic carbon (PIC_{Sed}) were calculated as the difference between TPC_{Sed} and POC_{Sed}. BSi_{Sed} and TPP_{Sed} concentrations were measured spectrophotometrically according to Hansen and Koroleff (1999), after subsampling ∼ 2 mg of the sediment. Prior to that, TPP_{Sed} samples were pressure-cooked in 40 mL of deionized water including an oxidizing agent (Oxisolv, Merck) and BSi_{Sed} samples were leached in 0.1 mol L^{-1} NaOH at 85 °C for 135 min to dissolve biogenic silicate, and the reaction was stopped with 0.05 mol L^{-1} H_2SO_4. The precision of BSi_{Sed} measurements was similarly estimated from the average standard deviation between duplicate measurements over the course of the experiment and amounted to ± 0.01 µmol BSi L^{-1} d^{-1}.

2.3.2 Water column particulate matter and photosynthetic pigments

For TPC / N_{WC}, POC / N_{WC}, and photosynthetic pigment analyses, subsamples were obtained by filtering water column material onto individual pre-combusted glass-fiber filters (0.7 µm, Whatman). Filters designated for POC / N_{WC} were acidified using 2 mol L^{-1} HCl for ∼ 2 min to remove inorganic carbon, while unacidified filters were collected for TPC / N_{WC}. Both sets were placed in pre-combusted glass petri dishes and dried overnight at 60 °C. All filters were packed in tin capsules (8 × 8 × 15 mm; LabNeed GmbH, Germany), stored in a desiccator, and returned to Kiel. There, carbon and nitrogen contents were quantified using a CN analyzer (Euro EA-CN, HEKAtech) following the procedure described for the sediment trap samples, and accuracy was likewise monitored by measuring acetanilide standards of known C and N content between samples. Routine duplicate measurements were not conducted for water-column particulate C / N, but suspect values were re-measured where possible and if re-measurements confirmed the original value, both measurements were averaged, if the original value was not reproduced, it was replaced by the new measurement. During the entire filtration for photosynthetic pigments (Chl *a*+ Fucoxanthin), light exposure was minimized by covering the filtration racks with aluminum-foil. Subsequently, filters were stored in 2 mL cryovials at −80 °C until further analysis. While Chl *a* was used as a broad indicator of total phytoplankton biomass, Fucoxanthin is an accessory pigment associated mainly with diatoms and was therefore used as a more specific proxy for diatom-associated

biomass and diatom contribution to bloom development (Roy, 2011). Pigment extraction was achieved using 100 % acetone (HPLC-grade, Merck) and a cell mill (Precellys, France) with glass beads (0.5 mm) for 30 s to limit sample heating during homogenization. Samples were centrifuged at 10 000 rpm (10 min, 4 °C) and the supernatant filtered through a 0.2 µm PTFE syringe filter (13 mm, Lab Logistics Group). Concentrations of Chl *a* and Fucoxanthin within the supernatant were determined using High-Performance Liquid Chromatography (Thermo Scientific HPLC Ultimate 3000) according to Van Heukelem and Thomas (2001) and peaks were calibrated using a library of premeasured commercial standards. Where applicable, Chl *a* outliers were corrected using fluorometer measurements. Subsamples for BSi_{WC} were filtered onto cellulose acetate filters (0.7 µm, Whatmann) and immediately stored at −20 °C. To dissolve the particulate silica, filters were leached in 0.1 mol L^{-1} NaOH at 85 °C the following day. After 135 min, leaching was terminated by adding 0.05 mol L^{-1} sulfuric acid. Dissolved silicate concentrations were then quantified spectrophotometrically following the procedure of Hansen and Koroleff (1999). Similar to TPC / N_{WC} and POC_{WC} measurements, potential outliers in water-column BSi measurements were re-measured where possible. If re-measurements confirmed the original value, both measurements were averaged, if the original value was not reproduced, it was replaced by the new measurement. Limits of detection were estimated from repeated blank measurements as the mean blank value plus three standard deviations, yielding 0.13 µmol L^{-1}.

2.3.3 Particle sinking velocities and porosities

Particle sinking velocities and porosities of sediment trap material were determined every two days by video-microscopy following methods described in Bach et al. (2012). Particles were imaged during gravitational sinking within a vertically mounted sinking chamber (cuvette 10 × 10 × 350 mm) positioned between a Raspberry Pi camera module (1920 × 1080 px; depth of field 1.5 mm) and a backlight. Sediment subsamples were diluted with 0.2 µm-filtered seawater (1 : 1–1 : 40, depending on particle density) and loaded into the chamber with a broad-tipped pipette. Measurements were conducted at in situ temperature (5 °C) in an airtight setup to minimize advection. Particles between 50–1000 µm were recorded for 20 min at 20 frames-per-second and 0.935 × magnification (3.274 µm px^{-1}). Several optical parameters allowed to identify multiple frames of a single particle during gravitational sinking. Prior to sinking velocity and porosity calculations, partially captured particles, or those out of focus were excluded based on python script (v3.9.18; Van Rossum, 2007 and openCV v4.6.0 Bradski, 2000) adjusted from Bach et al. (2012, for technical details see "Evaluation of sinking particles" in there). Subsequent sinking velocity and porosity calculations and data analysis was carried out using R-Studio (R Core Team, 2021) and ggplot2 (Wickham, 2016). Particle sinking velocities were calculated by applying a linear regression to their vertical position against time. Additionally, sinking velocities were corrected for temperature differences during measurements and for wall effects of the sinking chamber following (Ristow, 1997). Among the optical parameters acquired, equivalent spherical diameter (ESD) and image intensity (Int, grayscale range form 0–255) are established proxies to estimate particle porosity (Bach et al., 2019c), assuming more porous particles to transmit more light (higher grayscale values under backlit microscopy). To account for path-length effects, and larger particles typically being more porous than smaller ones (Laurenceau-Cornec et al., 2020), intensity was scaled with ESD to compute porosity:

$$\text{Porosity} = \left(\frac{\text{Int}}{255}\right)^2 \cdot \text{ESD} \quad (1)$$

Because marine particle size spectra are typically skewed towards smaller particles (Laurenceau-Cornec et al., 2020), we binned ESD into 50–100, 100–250, and 250–1000 µm (narrower bins for abundant small particles, broader for rarer large ones) and averaged sinking velocities and porosity within each bin. The 100–250 µm bin provided high particle count and the most informative signal for our analysis. It also matched the size of dominant aggregates observed from sediment trap material (Fig. S3), while also considered relevant for export processes (Clements et al., 2023; Puigcorbé et al., 2015). For clarity, we therefore focused on reporting exclusively this particle size class. We note that measurements were conducted ex situ; nevertheless, this approach has robustly tracked relative changes in particle dynamics in prior studies (Bach et al., 2019c; Baumann et al., 2021, 2023; Suessle et al., 2025).

2.3.4 Community Respiration

Community respiration data of the mesocosms experiment from Helgoland form part of a broader study on microbial metabolic rates under OAE and were provided by Marín-Samper et al., with methodological and data processing details provided in previous publications (Marín-Samper et al., 2024a, b). In brief, respiration rates were determined from oxygen consumption following the Winkler method and recommendations by Bryan et al. (1976), Carritt and Carpenter (1966) and Grasshoff et al. (1999). At each sampling day, mesocosm water collected in 4.5 L polycarbonate bottles was used to rinse and fill eight 125 mL soda-lime bottles per mesocosm via silicone tubing fitted with a 280 µm mesh ensuring overflow and checked to be bubble-free. Per mesocosm, four bottles were immediately fixed (1 mL $MnSO_4$ and 1 mL alkaline NaI) to determine initial oxygen concentrations, while four were incubated in the dark for 24 h (opaque bags) in an incubator continuously supplied with harbor water to maintain in situ temperature. Environmental conditions were logged using HOBO sensors (UA-

002-64, New Zealand) from 10–30 March (mean temperature: 8.43 ± 1.96 °C day; 8.02 ± 1.64 °C night; irradiance: ~ 0.20 µmol photons $m^{-2}\,s^{-1}$), but subsequent records were unavailable due to logger flooding. After incubation, remaining samples were fixed, allowed to settle for ≥ 2 h and acidified (1 mL of 5 mol L^{-1} H_2SO_4) prior to measurement. Oxygen concentrations were determined via titration with an automated colorimetric end-point detection (Dissolved Oxygen Analyzer, SIS, Germany), using 0.25 mol L^{-1} sodium thiosulfate ($Na_2S_2O_3 \times 5\,H_2O$). Community respiration (CR) rates were then calculated from the mean of the four replicates according to:

$$\mathrm{CR}\left(\mu\mathrm{mol\,L^{-1}h^{-1}}\right) = \frac{\mathrm{Conc_I} - \mathrm{Conc_D}}{h_\mathrm{D}} \quad (2)$$

where $\mathrm{Conc_I}$ and $\mathrm{Conc_D}$ represent the average oxygen concentrations of the initial and dark-incubated samples and h_D the incubation time in hours.

2.3.5 Bacterial Abundances

Bacterial abundances were provided by Antoni et al. (2025), and determined every two days from 2 mL cryovials containing mesocosm water previously fixed with formaldehyde (final concentration 1 %, 4 °C for 24 h, stored at −80 °C). Enumeration was conducted by flow cytometry (FACSCalibur, BD Biosciences, USA) following the bacterioplankton protocol of Marie et al. (1999). Prior to measurements, samples were stained with SYBR Green I (1 : 10 000) and incubated for 15 min in the dark. Data acquisition was performed for one minute, and prokaryotic populations were gated manually for each run using floreader.io. Cell concentrations were calculated from the number of gated events relative to the calibrated flow rate (µL min^{-1}). Instrument settings, gating images, and detailed workflows are publicly accessible via GitHub (https://github.com/Dom-Antoni/RETAKE_Analysis/tree/RETAKE-Microbiome, last access: 10 November 2025). Bacterial abundances were determined to derive a biomass-normalised proxy for microbial activity (Bac : Chl *a*), used to asses whether OAE-driven changes in heterotrophic carbon degradation during particle transit could account for observed shifts in sediment trap BSi : POC ratios.

2.3.6 Carbonate chemistry and nutrient concentrations

TA and DIC samples were collected with an overflow of approximately twice the target volume (500 mL), ensuring minimal air contact. Samples were analyzed at room temperature within 12 h of collection. To eliminate $\mathrm{PIC_{WC}}$, both TA and DIC samples were filtered through 0.2 µm filters (Whatman). TA was measured in technical duplicates by two-stage open-cell potentiometric titration using hydrochloric acid (0.05 mol L^{-1}) on a Compact Titrosampler 862 (Metrohm, Munich, Germany) with a built in PT1000 temperature sensor. DIC was determined in triplicates via infrared absorption with an AIRICA system (MARIANDA, Kiel, Germany) coupled to a differential infrared gas analyzer (LI-7000, LI-COR Biosciences GmbH, Germany). Both DIC and TA values were corrected against certified reference materials (batch no. 197; Dickson, 2010) to ensure accuracy and the precision of DIC and TA amounted to ± 1.9 and ± 2.0 µmol kg^{-1}, respectively. Additional carbonate system parameters were computed using the Excel-based CO_2SYS macro (Pierrot et al., 2021), applying water column–averaged temperature and salinity measurements from CTD profiles, as well as dissolved phosphorous and silicate concentrations for corrections. Carbonic acid dissociation constants K_1 and K_2 were taken from Sulpis et al. (2020), sulphuric acid from Dickson et al. (2007), hydrogen fluoride from Perez and Fraga (1987) and total boron from Lee et al. (2010). DIC and TA derived in situ pH_T was regressed against measured depth-integrated CTD pH to bring it on the total scale. Whenever outliers were detected DIC or TA carbonate chemistry speciation was calculated from the remaining parameter and CTD pH_T. Concentrations of dissolved inorganic nutrients ($NO_3^- + NO_2^-$, PO_4^{3-}, $Si(OH)_4$) were determined using UV-VIS spectrophotometry. Colorimetric analyses followed the procedures described Hansen and Koroleff (1999) and refractive index corrections were applied according to Coverly et al. (2012). The accuracy of nutrient measurements was monitored using certified reference material and precision was estimated from the average standard deviation between duplicates over the course of the experiment ($NO_3^- = \pm 0.1$ µmol L^{-1}, $NO_2^- = \pm 0.003$ µmol L^{-1}, $PO_4^{3-} = \pm 0.005$ µmol L^{-1}, $Si(OH)_4 = \pm 0.04$ µmol L^{-1}). Limits of detection were likewise estimated from repeated blank measurements as the mean blank value plus three standard deviations, yielding 0.03 µmol L^{-1} for PO_4^{3-}, 0.3 µmol L^{-1} for $Si(OH)_4$, and 0.5 µmol L^{-1} for NO_x ($NO_3^- + NO_2^-$).

2.4 Bloom analysis

To align comparisons of mesocosms on a common biological clock (i.e., trophic state), we identified phytoplankton bloom start and duration separately for each mesocosm using Chl *a* dynamics. Although treatment-induced shifts in bloom timing are relevant to OAE environmental safety, a calendar-day fixed analysis would inadvertently mix bloom and non-bloom days across mesocosms and blur differences in OAE-mediated biomass build-up and stoichiometry. From sampled Chl *a* concentrations, short-term variability was reduced using a centered 3-sampling-day moving average (note: for the delayed treatment, top and bottom layers were averaged on days 5–6). A mesocosm-specific baseline (B) was defined as the median of smoothed Chl *a* values during days 1–6. Bloom detection started on day 7, after full treatment manipulation was achieved. Bloom start was defined as the first of two consecutive sampling days in which (i) smoothed

Chl *a* exceeded a baseline-relative threshold on both days: Chl $a \geq (1+\alpha)\cdot$B (with $\alpha = 0.35$ and B = baseline), and (ii) day-to-day slopes of the smoothed Chl *a* series were positive on both days. Bloom end was determined only after the main Chl *a* peak and was defined as the first of two consecutive sampling days in which (i) smoothed Chl *a* fell back to Chl $a \leq (1+\beta)\cdot$B on both days (with $\beta = 0.70$, and again B = baseline), and (ii) at least one day had a negative slope. Separate start and end thresholds were used to provide hysteresis (with $\alpha < \beta$). Among various tested combinations of α- and β-values the selected pair preserved sensible fit to the observed bloom-patterns of smoothed and raw Chl *a* within all treatments. To further evaluate how well the selected thresholds captured bloom development across mesocosms, we compared the threshold-defined bloom window with a reference bloom window around each mesocosm's Chl *a* peak, which was bounded by the minima before and after the peak. For both windows, we calculated the area under the Chl *a* curve (termed AUC) and expressed the ratio of these areas ($AUC_{\alpha\,/\,\beta}$ / $AUC_{reference}$) as AUC_m %. This metric was used to assess how completely the threshold-based method captured each mesocosms bloom. A detailed visualization of the analysis per mesocosm can be found in Fig. S4, providing raw and smoothed Chl *a* values, baselines and thresholds, defined start and end days per mesocosm, as well as AUC_m % diagnostics. All analyses were conducted in R (R Core Team, 2021) using the "zoo" package (Zeileis and Grothendieck, 2005) for centred 3 d smoothing and windowed run tests (rollapply), and ggplot2 (Wickham, 2016) for visualization.

2.5 Sediment deposition analysis

Sediment deposition events may not only occur at different points in time relative to the bloom start but could also exhibit different durations. Analysing sediment deposition on fixed calendar days would therefore distort estimates of export magnitude and stoichiometry. Similarly to water column blooms, we identified sediment deposition events per mesocosm to align comparisons on a common biological clock and accommodate variation in the coupling of production and export. Daily POC fluxes were used to quantify sediment deposition events. Cumulative export was calculated by summing daily fluxes to the end of the experiment, and short-term variability was reduced using a centred 3-sampling-day moving average. From there, we calculated the day-to-day slopes (m) of the smoothed cumulative curve, which served as a deposition intensity proxy. Event detection was restricted to a mesocosm-specific search window beginning at the day of water column bloom onset and ending at the day of bloom termination $+w$ (an extension to the search window). To remove continuous background deposition before bloom-driven export, a baseline slope (m_B) was defined as the median slope from days ≥ 5 and $<$ bloom onset, and relative deposition intensity was defined as $m_{rel} = m - m_B$. For each mesocosm, event detection was centred around the day of maximum relative intensity (m_{max}), representing peak deposition. Deposition event start was defined as the first day within the search window where $m_{rel} \geq \alpha \cdot m_{max}$ and the end of events as the day on which $m_{rel} \leq (1-\alpha)\cdot m_{max}$ (note, end detection was only allowed after m_{max} and water column bloom end). After testing several α and extended search windows (w) combinations, we chose $\alpha = 0.32$ and $w = 6$ d. The combination yielded start and end days consistent with the observed phenology of cumulative POC flux and slope time series. To further evaluate the chosen α- and w-combination capturing the deposition events, we compared two metrics: (a) the cumulative flux captured by the detected event window relative to total cumulative flux over the experiment, and (b) flux density, defined as the captured cumulative flux divided by the event duration in days. Here, we note that mesocosms with secondary blooms and associated secondary deposition pulses had a lower proportion of total cumulative flux captured within the detected event, reflecting export distributed across multiple pulses rather than a failure of event detection; this did not affect our OAE analysis, as treatment comparisons were based on averages of the first bloom and associated deposition event. Detailed per-mesocosm visualization of the analysis can be found in Fig. S5, providing raw and smoothed cumulative POC flux values, slopes, detected start, end and peak deposition days, as well as proportion of total flux captured and flux density. Analyses were conducted in R (R Core Team, 2021) using the "zoo" package (Zeileis and Grothendieck, 2005) for centred 3 d smoothing and windowed run tests (rollapply), and ggplot2 (Wickham, 2016) for visualization.

2.6 Statistical analysis

To assess OAE effects on biogeochemical water-column and sediment parameters, daily responses (i.e., sampling days) were either averaged or summed up (for cumulative fluxes), yielding a single independent estimate per mesocosm for each analysis window (bloom phase, deposition event, or last experimental day as cumulative endpoint). Linear models were then fitted (across dilution scenarios) using measured in situ mean pH_T as the primary explanatory variable. Where relevant, we also ran parameter regressions, including cross-phase fitting, linking bloom and sediment deposition averages. This allowed us to estimate effect sizes of within phase relationships and disentangle drivers of production–export coupling. Model assumptions were checked prior to analysis, i.e., linearity (residual–fitted plots and Reset test), homoscedasticity (scale-location plots and Breusch–Pagan test) and normality of residuals (qq-plots and Shapiro–Wilk test) with base R and the lmtest package (R Core Team, 2021; Zeileis and Hothorn, 2002). Whenever model assumptions were violated, either data transformations were applied, or outliers were flagged visually in figures and noted in statis-

tical tables (Table S1). All plots, including diagnostics, were produced using ggplot2 (Wickham, 2016).

3 Results

3.1 Carbonate chemistry and nutrient conditions under increasing OAE

Deployment of unequilibrated OAE across varying dilution scenarios was successful, achieving target alkalinity post-mixing (Figs. 1b, S3). Carbonate saturation states ($\Omega_{Ca\,/\,Ar}$) remained high after mixing and carbonate precipitation was triggered in the two highest alkalinity mesocosms from mid-experiment onwards, decreasing TA and pH_T (Fig. S2) and yielding high, threshold-like PIC fluxes in respective mesocosms. However, this did not confound results, as analyses were based on measured pH_T (not target levels) and carbonate formation neither directly altered organic export magnitude, nor indirectly via increased particle sinking velocities (Fig. S6, Table S1). Additionally, blooms of comparable magnitude occurred regardless (Fig. 2a, c). This is consistent with prior observations, and we refer to Suessle et al. (2025) for a detailed discussion of OAE-driven carbonate precipitation and its effect on biological carbon sequestration. While CO_2 increased from carbonate precipitation and atmospheric ingassing, the rise in fCO_2 over the experiment was relatively small in the two highest mesocosms (Fig. S2b, d). CO_2 levels closely tracked initial treatment spacing at $\Delta TA \geq 750\,\mu mol\,kg^{-1}$, generally remaining below 50 µatm (down to $fCO_2 < 15$ µatm and $pH_T > 9.25$). Bloom-driven CO_2 drawdown was small and only evident under ambient or moderate alkalinity increases (Fig. S2). Initial nutrient conditions reflected typical North-Sea spring conditions (Wiltshire et al., 2010) and were sufficient to support ample biomass growth ($Si \approx 14.5\,\mu mol\,L^{-1}$, $NO_3^- \approx 17.7\,\mu mol\,L^{-1}$, $PO_4^{3-} \approx 0.05\,\mu mol\,L^{-1}$, Fig. S7). Increased alkalinity treatments initially showed slowed nutrient drawdown but did not alter overall consumption consistently (Fig. S7, Table S1) which closely followed bloom development throughout the experiment. Because sediment traps integrated particle signals from both initially alkalized and initially unalkalized layers, and because main export responses were directionally consistent across dilution scenarios (Fig. 3e), the common pH_T gradient was retained as the primary focus of the export analysis (see Sect. 2.1). Mesocosms with similar alkalinity levels were therefore treated as duplicates, while original treatment colors were retained for transparency. Further, we focus here on water column driven export dynamics, while general carbonate-chemistry feedback and bloom-timing effects, relevant to OAEs environmental safety, are addressed elsewhere (Tammen et al., 2026).

3.2 Water column biomass and silica ballasting ratios

Across mesocosms, the calculated bloom onset and termination based on Chl *a* dynamics captured 95 ± 2.7 % (mean $\pm$ SD) of the total biomass standing stocks (Fig. S4). Start and end days varied between day 7 and 15, and day 15 and 35, respectively, with earlier bloom onset and termination in the low- to intermediate-alkalinity treatments and the latest onset and termination in the highest-alkalinity treatments (details in Fig. S4). Within blooms, averaged phytoplankton biomass metrics (Chl *a* and POC_{WC}) were not affected by the OAE induced pH_T-gradient and displayed similar concentrations (Fig. 2b, c, Table S1). Averaged Chl *a* concentrations varied between 5.7 and 3.5 $\mu g\,L^{-1}$ and POC_{WC} concentrations between 42.7 and 27.8 $\mu mol\,L^{-1}$ (Fig. 2b, c). Fucoxanthin, a diatom-associated accessory pigment used as a proxy for diatom biomass (see Sect. 2.3.2), tracked temporal Chl *a* dynamics (Fig. 2a, d), indicating diatom-driven bloom development, and was likewise not affected by pH_T (Fig. S8, Table S1). In contrast, water column biogenic silica concentrations (BSi_{WC}) within blooms declined with increasing pH_T, by 40 % from 5.5 to 3.3 $\mu mol\,L^{-1}$ and water column silica ballasting ratios ($BSi_{WC} : POC_{WC}$) halved from 0.16 to 0.08 mol : mol (Fig 2e, f, Table S1). Over time, POC_{WC} concentrations generally remained elevated after build-up, albeit some variability, but BSi_{WC} concentrations showed a consistent rise followed by a pronounced decline across all mesocosms (Fig. S8). Consequently, water-column silica ballasting ratios ($BSi_{WC} : POC_{WC}$) decreased over the course of the experiment.

3.3 Sediment silica ballasting ratios decline across the pH_T gradient

Sediment deposition following bloom events in each mesocosm ranged between 37 % and 81 % of total export, varying with distinct deposition dynamics (e.g., secondary pulses following secondary blooms, Fig. S5). The onset of deposition lagged blooms by 3.5 ± 3.0 d (mean $\pm$ SD, details in Fig. S5), indicating tight but varying coupling of production and export of biomass, and showed no systematic delay under OAE. Within the defined deposition events, averaged POC and BSi flux magnitudes showed no detectable pH effect (Fig. 3b, d, Table S1), ranging from 6.2 to 2.2 $\mu mol\,L^{-1}\,d^{-1}$ and from 1.2 to 0.6 $\mu mol\,L^{-1}\,d^{-1}$, respectively. In general, sediment-trap BSi fluxes were positively correlated with water column BSi production (Fig. S9, Table S1). Likewise, POC and BSi fluxes correlated positively (Fig. S9, Table S1) and followed temporal patterns similar to water column Chl *a* dynamics, but with the previously noted delay and more episodic, less uniform peaks (compare Figs. 2a; 3a, c). In contrast, sediment silica ballasting ratios ($BSi_{Sed} : POC_{Sed}$) declined sharply with increasing pH_T: deposition-averaged values fell by 60 % from 0.27 to 0.10 mol : mol, while daily ratios decreased over time (Fig.

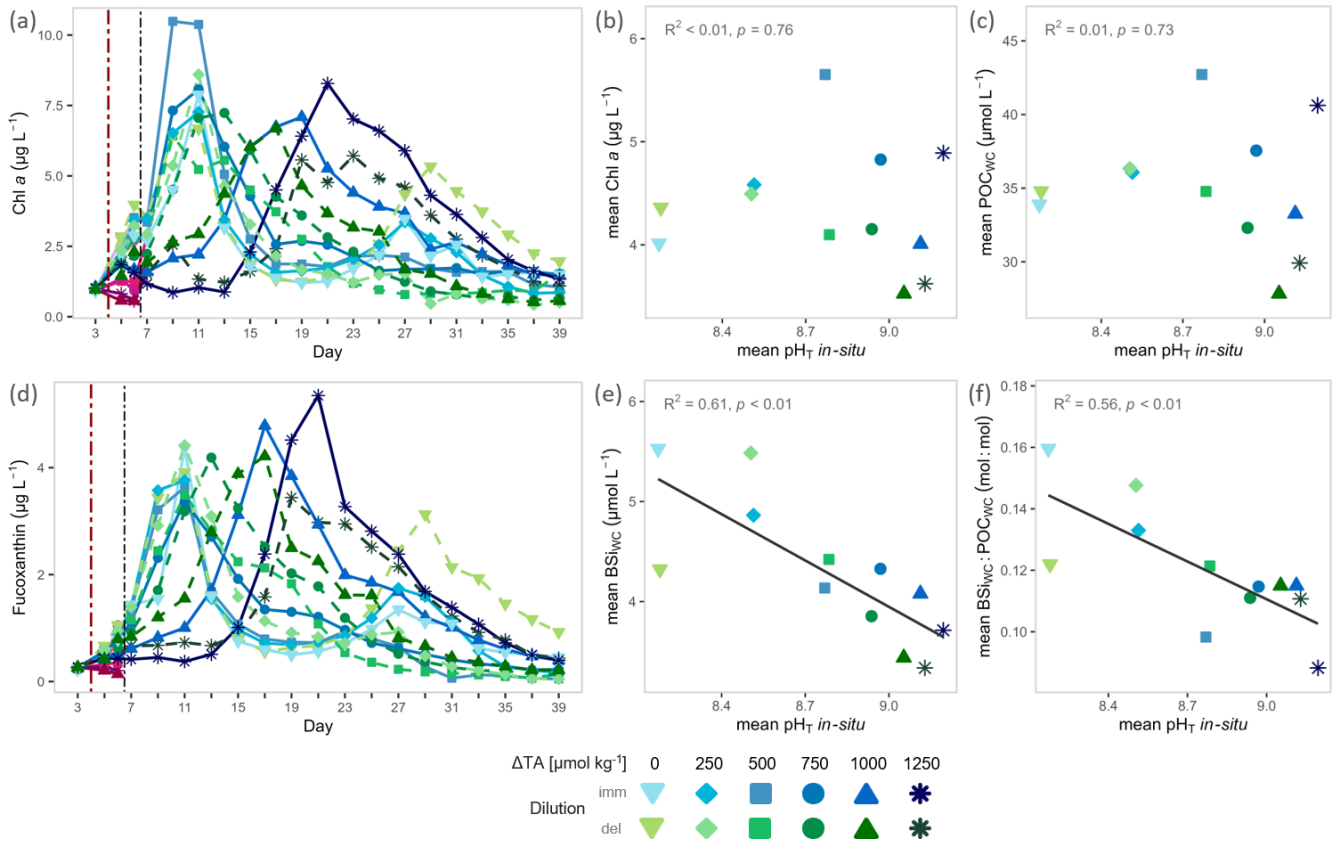

Figure 2. Phytoplankton biomass and silica ballasting ratios under OAE. Temporal trajectories of **(a)** chlorophyll *a* (Chl *a*) and **(d)** Fucoxanthin concentrations. pH-gradient responses of bloom-window averages for **(b)** Chl *a*, **(c)** POC_{WC}, **(e)** BSi_{WC}, and for **(f)** water column silica ballasting ratio ($BSi_{WC} : POC_{WC}$). Note: The averaging windows for pH_T and each response variable differ among mesocosms, defined by the identified bloom window per mesocosm (see Sect. 2.4 and Fig. S4). Pink–purple symbols represent surface-layer measurements from delayed-dilution mesocosms on days 5–6; hue encodes the alkalinity addition (ΔTA, $\mu mol\,kg^{-1}$), with darker purple indicating higher ΔTA. The red dash-dotted vertical line marks the start of the alkalinity manipulation; the black dash-dotted line marks completion by mixing via the sediment trap. Grey annotations report statistical tests (see details in Table S1).

3e, f, Table S1). Other deposition-averaged fluxes (TPN, TPP) and experiment-integrated cumulative fluxes of all major elements were unaltered by OAE (Figs. S10, S11, Table S1). This confined the sediment signal to (a) a compositional change rather than changes in bulk flux, and (b) post-bloom deposition pulses, rather than continuous export.

Notably, silica ballasting ratios (BSi : POC) increased from the water column to the sediment trap, rising approximately twofold at ambient alkalinity with diminishing enrichment as alkalinity increased (Fig. 4a, comparing Fig. 2f and 3f). Accordingly, sediment and water column silica ballasting ratios correlated, but exceeded a 1 : 1 scaling: each mol : mol decrease in $BSi_{WC} : POC_{WC}$ corresponded to a 1.73 mol : mol decrease in $BSi_{Sed} : POC_{Sed}$ (slope $= 1.73$, Table S1). Additionally, particle porosity in the 100–250 µm size class increased consistently with alkalinity-driven pH_T (Fig. S10, Table S1), and negatively correlated with sediment silica ballasting ratios (Fig. 4b, Table S1). These porosity changes, however did not translate into systematic changes in particle sinking velocities (Fig. S9; Table S1), which in general were unaffected by pH_T, aside from higher velocities under the highest alkalinity treatments (Fig. S10; Table S1). Consistent with this decoupling, sinking velocities also did not scale with either water column or sediment silica ballasting ratios (Fig. S9; Table S1). Finally, we found no evidence for enhanced POC remineralization as Chl *a*-normalized community respiration and bacterial abundances were unaffected by pH_T and did not scale with particle porosity (Fig. S12, Table S1).

4 Discussion

This study shows that diatom-derived silica ballasting ratios in sediment material ($BSi_{Sed} : POC_{Sed}$) decreased by 60 % across the applied alkalinity-induced pH_T gradient. Given the pivotal role of diatoms in global carbon sequestration (Brzezinski et al., 2015; Le Moigne et al., 2012; Ragueneau et al., 2006; Tréguer et al., 2018), our results indi-

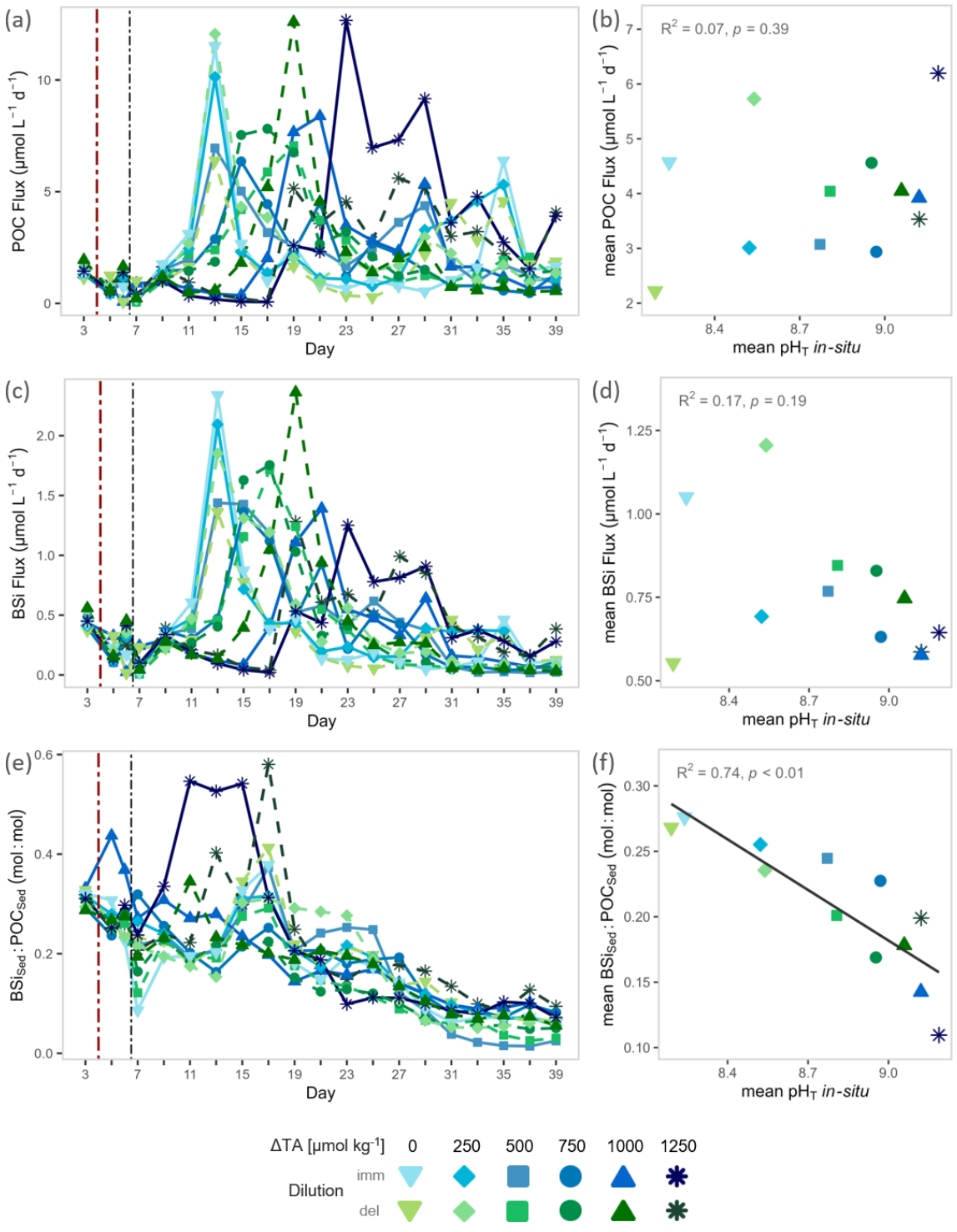

Figure 3. Organic matter export and silica ballasting ratios under OAE. Temporal trajectories of **(a)** particulate organic carbon export (POC Flux), **(c)** biogenic silica export (BSi Flux), and **(e)** sediment silica ballasting ratio ($BSi_{Sed} : POC_{Sed}$). pH-gradient responses of deposition-window averages for **(b)** POC flux, **(d)** BSi flux, and **(f)** sediment silica ballasting ratio ($BSi_{Sed} : POC_{Sed}$). Note: The averaging windows for pH_T and each response variable differ among mesocosms, defined by the identified deposition window per mesocosm (see Sect. 2.5 and Fig. S5). The red dash-dotted vertical line marks the start of the alkalinity manipulation; the black dash-dotted line marks completion by mixing via the sediment trap. Grey annotations report statistical tests (see details in Table S1).

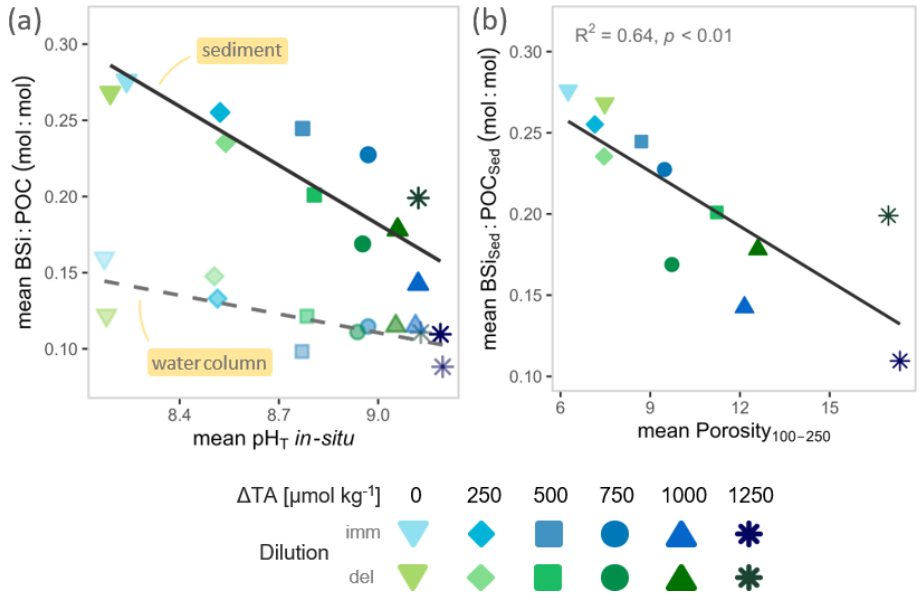

Figure 4. Enrichment of silica ballasting ratios and links to particle structure. **(a)** Visualizing export-phase intensification of silica ballasting ratios across the pH_T gradient via variable slopes; dark solid regression line + opaque symbols = sediment, light dashed regression line + transparent symbols = water column. **(b)** Parameter regression within deposition phase for sediment silica ballasting ratio vs. mean particle porosity (in 100–250 µm size class). Note: To link processes across phases, sediment parameters ($BSi_{Sed} : POC_{Sed}$, $Porosity_{100–250}$) were averaged over each mesocosm's deposition window, whereas water column silica ballasting ratios ($BSi_{WC} : POC_{WC}$) was averaged over each mesocosm's bloom window; for **(b)** pairs were matched by mesocosm for regression. Both, bloom and deposition windows (and thus averaging days) differ among mesocosms (see Sect. 2.4, 2.5; compare Figs. S4 and S5). Grey annotations report statistical tests (see details in Table S1).

cate that OAE-driven pH_T increases can modify biological-pump functioning in ways that are relevant for net CO_2 removal estimates. Below, we outline plausible processes driving changes in the build-up and export of silica while recognizing that multiple processes can co-occur in multi-factorial mesocosm experiments.

4.1 pH-enhanced silica dissolution decouples ballasting from biomass build up

Within bloom phases, average BSi concentrations and water column silica ballasting ratios ($BSi_{WC} : POC_{WC}$) declined across the alkalinity-induced pH_T gradient, despite unchanged bloom magnitudes (Chl a, POC_{WC}) across treatments. Notably, the decoupling of silica from bulk biomass was even more pronounced in sinking compared to suspended material. Together, these observations suggest enhanced BSi dissolution at higher pH_T. Because seawater is generally under-saturated with respect to silica (Lewin, 1961), dissolution rates can be substantial, reaching up to 43 % of gross production rates during blooms (Beucher et al., 2004). Moreover, dissolution rates are known to increase at higher pH (Brady and Walther, 1989; Socratis et al., 2008; Van Cappellen et al., 2002), due to facilitated hydrolysis of siloxane bonds at the frustule surface (Barker et al., 1994). In line, $BSi_{Sed} : POC_{Sed}$ exhibited a steeper decline across the applied pH_T gradient (Fig. 4a, see slopes in Table S1), suggesting that silica loss intensified during particle transit. Living diatoms protect their frustules with organic coatings (Lewin, 1961; Van Cappellen et al., 2002), but upon senescence (i.e., bloom termination and export), bacterial degradation of these coatings strongly accelerates pH-enhanced BSi dissolution (Bidle and Azam, 1999). Given the higher dissolution rates in older material, our results are consistent with chemically controlled BSi loss, as silica frustules lose their coatings and become increasingly susceptible to pH-driven hydrolysis during transit. This mechanism could explain the observed decline in water column silica ballasting ratios ($BSi_{WC} : POC_{WC}$) by up to 50 % per unit increase in pH, a number consistent with chemical studies reporting a 60 %–70 % per-unit-pH sensitivity of dissolution rates (Dove and Elston, 1992; Greenwood et al., 2005). Additionally, the global-scale pH sensitivity of BSi dissolution was estimated by Taucher et al. (2022), who reported a 17 % increase in export Si : N under an approximate pH decline of 0.3 units (under end-of-century RCP 8.5 scenarios). Scaled to a full pH unit, this corresponds to an estimated 56 % decrease in dissolution and, despite the opposite sign of the perturbation, falls within our estimate of up to 60 % increase in dissolution per unit pH increase (measured from $BSi_{Sed} : POC_{Sed}$). The convergence of these independent estimates, derived from contrasting pH perturbations across different ecosystems and

experimental approaches, further supports a view of chemically controlled, pH-sensitive BSi dissolution as a general and broadly applicable mechanism.

Although our experiment was conducted in a coastal system, the mechanism proposed here may extend beyond such regions if the observed BSi loss is primarily governed by pH-enhanced dissolution. This is particularly relevant given recent global OAE-efficiency estimates: Zhou et al. (2025) showed that OAE efficiency varies strongly with latitude and season, identifying high latitudes around $\sim 50^\circ$ N and $\sim 50^\circ$ S, including parts of the North Pacific and Southern Ocean, as favourable deployment locations due to enhanced surface retention of added alkalinity and efficient air–sea CO_2 equilibration. Yet, these regions are also among the most relevant globally for seasonal diatom-driven carbon export (Le Moigne et al., 2012, Ragueneau et al., 2006). Taucher et al. (2022) further identified these regions as highly sensitive to pH-driven silica preservation under ocean acidification, suggesting they may also be particularly susceptible to silica dissolution under OAE. Importantly, Zhou et al. (2025) estimated OAE efficiency primarily from physical–chemical controls while assuming negligible biogeochemical feedbacks from carbonate-chemistry changes. Such maps therefore provide an essential baseline, but not necessarily a complete estimate of retained net CO_2 sequestration under OAE. Our findings suggest this distinction matters in highly productive, diatom-dominated systems, where OAE-driven BSi dissolution could weaken silica ballasting and potentially alter biological-pump efficiency. However, whether this translates into a net reduction in CO_2 sequestration will depend on how dissolution-derived DSi is redistributed within the water column and on its role in regulating diatom growth.

Despite the relevance of this mechanism, recent OAE work has documented changes in DSi drawdown and BSi dynamics (Ferderer et al., 2022; Gately et al., 2023; Paul et al., 2025), but direct evidence for impacts on BSi dissolution under OAE still remains limited, particularly along the sinking pathway. A key distinction of our experiment was the strong carbonate-chemistry perturbation ($pH_T > 9.25$) extending beyond the range typically tested to date ($pH_T = 8.2$–9.0; Ferderer et al., 2024, 2025; Gately et al., 2023; Guo et al., 2024, 2025; Li et al., 2024; Suessle et al., 2025), across a highly resolved gradient (duplicated, six alkalinity levels). Smaller perturbations would inherently reduce pH-sensitive dissolution and, with fewer treatment levels and/or replication, make subtle responses harder to distinguish from background variability. Detectability is further constrained by smaller or inconsistent blooms, reported in many studies (1–5 µg Chl $a\,L^{-1}$; Ferderer et al., 2024; Guo et al., 2024; Kousoulas et al., 2025; Suessle et al., 2025), whereas our experiment consistently reached above 7.5 µg Chl $a\,L^{-1}$. Higher biomass likely increased signal-to-noise ratios by leveraging dissolution changes and in combination with the long experimental duration, allowing for a full bloom progression in all treatments (onset to export). Critically, our clearest fingerprint emerged when separating suspended from sinking material, with the pH signal intensifying during transit (Fig. 4a), shown by > 1 slope when scaling $BSi_{WC} : POC_{WC}$ with $BSi_{Sed} : POC_{Sed}$ (Table S1). Although vertical transport may be less pronounced in dynamic coastal systems, the signal observed over only 3 m transit may represent a conservative estimate of dissolution along longer sinking pathways. Studies focusing only on suspended pools or production metrics (Ferderer et al., 2025; Gately et al., 2023; Subhas et al., 2022), would miss the export-phase intensification, leaving the signal too weak to detect in the suspended fraction. Notably, reduced water column BSi at otherwise similar biomass build-up, has been reported for a diatom-dominated OAE experiment ($pH \approx 8.6$; Ferderer et al., 2022), though the authors could not resolve the responsible mechanism. Moreover, their signal did not propagate into sediment-trap material, potentially because of the lower export magnitudes as well as sampling frequency compared to our study, likely limiting the detectability due to noise. Similarly, a related analysis of the present experiment did not detect a clear fCO_2 effect on bloom-phase water-column BSi concentrations. This is not necessarily inconsistent with our results, as that analysis used a broader suite of water-column parameters to define bloom phases, resulting in different bloom-phase windows, and retained the initial dilution-scenario grouping. In addition, fCO_2 and pH emphasize different aspects of the OAE perturbation, reflecting e.g., carbon-availability constraints for phytoplankton or pH-dependent chemical processes such as silica dissolution, respectively. These differences further emphasize that the detectability of silica-related OAE responses can depend on both temporal and analytical framing. Finally, although the OAE studies discussed here span diverse ecosystems, ocean-acidification work has shown that the pH sensitivity of silica dissolution is global (Taucher et al., 2022). It further supports the directionality implied here and suggests that null results under OAE may instead reflect limited pH-range forcing and/or resolution, both statistical and methodological, rather than the absence of a dissolution response.

Although the decline in water column and sediment BSi : POC ratios suggests enhanced pH-driven silica dissolution, we note that a corresponding increase or hampered drawdown of dissolved silicate (DSi) was not detectable from water column concentrations. The signal was likely obscured by rapid re-assimilation during bloom phases, with treatment-specific differences in bloom dynamics (exponential vs. gradual development) further masking its detectability. Additionally, DSi enrichment within pore-water of sinking aggregates, likely a substantial fraction of dissolution-derived silica, did not contribute to water column measurements and was also not quantified from sediment trap samples, hindering silicon mass-balance approaches. Together, these constraints limited our ability to resolve dissolution signals from water column DSi alone, although we acknowl-

edge that enhanced silica regeneration certainly occurred and is mechanistically implied by the observed BSi losses.

4.2 Constraints on alternative drivers of silica ballasting losses

Although our results strongly suggest pH-driven chemical control of silica dissolution, we evaluated whether other production-side (silicification, community composition) or export-side (remineralization, sinking time) processes could alternatively explain the BSi : POC response under OAE. Physiologically, higher pH could in principle impede silicification by maintaining higher Si solubility and steepening the pH gradient that diatoms must overcome within their silicification compartments (Martin-Jézéquel et al., 2000; Vrieling et al., 1999). However, direct experimental evidence under OAE is still scarce (Ferderer et al., 2024, 2025; Gately et al., 2023; Oberlander et al., 2025), and responses under acidification are inconsistent, with silicification reported to both increase and decrease (Hervé et al., 2012; Petrou et al., 2019). While we did not directly quantify per-cell silicification, it is generally thought to increase at lower growth rates (Martin-Jézéquel et al., 2000; Timmermans et al., 2004). In our experiment, however, Chl *a* dynamics suggest that diatom growth decreased at higher alkalinity (early exponential vs. delayed gradual bloom development) consistent with our alkalinity perturbations reducing CO_2 to long-known growth-limiting levels ($\sim 1\,\mu mol\,kg^{-1}$, $fCO_2 < 15\,\mu atm$; Raven, 1993; Riebesell et al., 1993). In summary, these production-side considerations argue against a simple, uniform decline in species-level silicification to explain the observed decline in water column silica ballasting.

Further, community shifts could reduce water column silica ballasting ratios if OAE favored e.g., fewer diatoms relative to non-silicifying taxa, or more lightly silicified diatom species. Yet, evidence that OAE consistently drives community changes of sufficient magnitude to generate the strong $BSi_{WC} : POC_{WC}$ signals observed remains limited (Groppelli et al., 2026; Guo et al., 2024; Li et al., 2024; Subhas et al., 2022; Xin et al., 2024). While we did not resolve taxonomic composition or diatom size spectra, ocean-acidification studies have shown, that elevated fCO_2 can favor larger diatoms, a pattern attributed to alleviated diffusive CO_2 limitation and downregulation of energetically costly CCMs with increasing cell size (Bach and Taucher, 2019; Rost et al., 2008; Sommer et al., 2015; Wu et al., 2014). By extension, CO_2 limitation under unequilibrated OAE could bias competitiveness towards smaller taxa, consistent with Kousoulas et al. (2025), identifying specific larger diatom species as losers under unequilibrated OAE (low fCO_2). In a system typically dominated by large diatoms (Wiltshire et al., 2010) and subjected to CO_2 limitation exceeding its natural variability (Kirchner et al., 2020), such a competitive shift could be clearly expressed as a restructuring toward smaller diatoms. Yet smaller diatoms are generally thought to be more heavily silicified (per cell; Ragueneau et al., 2006; Sarthou et al., 2005), which at similar bloom magnitudes (see Chl *a*, POC_{WC}) would predict higher BSi per carbon biomass; this directionality directly opposes our observations, reinforcing pH-driven BSi dissolution as the dominant explanation. However, we acknowledge, that community shifts remain a plausible contributor to observed water column $BSi_{WC} : POC_{WC}$ signals, but they would not explain why the strongest decline in silica ballasting ratios occurs in exported material.

Lastly, changes in microbial carbon remineralization or particle sinking time could in principle alter sediment trap silica ballasting ratios ($BSi_{Sed} : POC_{Sed}$). Because organic carbon remineralization proceeds faster than silica dissolution, exported particles typically become enriched in BSi relative to POC with depth (Armstrong et al., 2001; Karakuş et al., 2025; Ragueneau et al., 2006). Consistently, we observed a two-fold enrichment of BSi : POC from the water column to the sediment trap at ambient alkalinity, but this enrichment was significantly reduced at higher alkalinity. Such a pattern would require systematic pH-driven changes in remineralization rates and/or residence time during sinking (i.e., sinking velocities). However, biomass-normalized remineralization proxies (CR : Chl *a*, Bac : Chl *a*) showed no systematic variation with pH, nor with particle porosity, known to enhance bacterial remineralization during transit (Grossart and Ploug, 2001; Ploug et al., 2002). Likewise, particle sinking velocities showed no consistent relationship with pH (aside from the pronounced increase associated with carbonate precipitation) and were not systematically related to porosity, also known to influence settling speed (Azetsu-Scott and Passow, 2004; Bach et al., 2019c). Thus, export-side changes in organic carbon remineralization metrics or sinking time were not apparent in our dataset. Taken together, the evaluated production- and export-side alternatives are not consistent with the observed direction and magnitude of the silica ballasting ratio (BSi : POC) response, further supporting pH-driven BSi dissolution to be the most likely explanation.

In addition to pH, we would like to extend our considerations to particle-quality traits. Aggregate microenvironments may modulate BSi dissolution during export. Higher aggregate porosity can enhance porewater exchange, which has been linked to elevated BSi dissolution in sinking particles (Moriceau et al., 2014; Passow et al., 2003). BSi dissolution kinetics are hampered by DSi accumulation in aggregate porewater, suppressing dissolution relative to freely suspended diatom frustules (Moriceau et al., 2007), with the net effect of porosity depending on the balance between porewater exchange and Si-solute build-up. In our mesocosms, porosity of sediment-trap particles increased along the alkalinity-induced pH gradient during bloom-following deposition events. Although we cannot quantify how strongly porosity contributed to BSi dissolution, the tight covariation between porosity and $BSi_{Sed} : POC_{Sed}$ (Fig. 4b) suggests that particle-quality traits may provide an additional control on export-phase BSi loss, and could modulate the pH signal.

5 Implications and Outlook

Our results indicate that OAE may decrease silica ballasting ratios via pH-enhanced BSi dissolution. In our experiment, higher pH reduced BSi : POC ratios most clearly in exported material, implying that a smaller fraction of carbon is transported to depth before remineralization. Such shoaling of remineralization would shorten carbon-sequestration timescales and shift nutrient regeneration upward in the water column. Enhanced dissolution would also regenerate DSi in the upper ocean, with context-dependent consequences for carbon export: in silicate-limited systems, regenerated DSi may sustain diatom production and partly buffer ballasting losses, whereas in Si-replenished systems weaker silica ballasting would more directly reduce carbon sequestration potential. The magnitude and potentially even the sign of these feedback may further depend on co-factors that modulate silicification and export efficiency, such as iron availability in the open ocean. Ecologically, dissolution-driven increases in upper-ocean DSi availability could also reshape phytoplankton community structure, with cascading effects on aggregation, grazing, and energy transfer to higher trophic levels, including fish. Together, these interacting feedback imply that OAE impacts on export and food-web transfer efficiency may be non-linear and ecosystem specific. Future OAE work should therefore constrain pH-driven silica dissolution across contrasting ecosystems and seasons, explicitly resolving suspended versus sinking pools and accounting for bloom versus background states, to identify where OAE can be applied without unintentionally weakening the biological carbon pump.

Data availability. The datasets presented in this study can be found in PANGAEA: https://doi.org/10.1594/PANGAEA.992023 (Suessle et al., 2026), https://doi.org/10.1594/PANGAEA.986507 (Schulz et al., 2025), https://doi.pangaea.de/10.1594/PANGAEA.987501 (Tammen et al., 2026).

Supplement. The supplement related to this article is available online at https://doi.org/10.5194/bg-23-4691-2026-supplement.

Author contributions. (in no particular order) Study design and conceptualization: PS, KS, MB, LK, UR, Sampling and laboratory analysis: PS, JS, JKT, LK, LMS, KS, Data analysis and interpretation: PS, NS, MB, JBR, KS, Writing (original draft): PS, KS, JBR, Writing (reviewing and editing): PS, with comments from all co-authors.

Competing interests. The contact author has declared that none of the authors has any competing interests.

Disclaimer. Publisher's note: Copernicus Publications remains neutral with regard to jurisdictional claims made in the text, published maps, institutional affiliations, or any other geographical representation in this paper. The authors bear the ultimate responsibility for providing appropriate place names. Views expressed in the text are those of the authors and do not necessarily reflect the views of the publisher.

Acknowledgements. We would like to thank the staff of the Biological Institute Helgoland (BAH), Alfred Wegener Institute, Helmholtz Centre for Polar and Marine Research, for access to facilities and for logistical support during the experiment. Also, we are grateful to Andrea Ludwig, Jana Meyer, Jan Hennke, and Anton Theileis for technical and organizational assistance, and to the KOSMOS Scientific Diving and Maintenance Team, Michael Sswat, Carsten Spisla, and Daniel Brüggemann, for essential diving support. At last, we would also like to thank Jule Ploschke for extensive help in the onsite export-laboratory, as well as Levka Hansen and Kerstin Nachtigall for laboratory assistance in Kiel. We would also like to thank Dominik Antoni and Svetlana Petric for providing bacteria count and fucoxanthin data, respectively.

Financial support. This study was funded by the Federal Ministry of Education and Research of Germany (BMBF) in the framework of RETAKE (grant/award nos. 03F0895A and 03F0895B), one of the six research consortia of the German Marine Research Alliance (DAM) research mission "Marine carbon sinks in decarbonisation pathways" (CDRmare). Additional support was provided through the Ocean Alk-Align project, funded by Carbon to Sea and the Thistledown Foundation. More support came from the Fundação para a Ciência e a Tecnologia (FCT, Portugal) with the reference UIDB/00153/2020. JBR is supported by FCT, within Contrato-Programa, Apoio Institucional, Portugal.

The article processing charges for this open-access publication were covered by the GEOMAR Helmholtz Centre for Ocean Research Kiel.

Review statement. This paper was edited by Koji Suzuki and reviewed by two anonymous referees.

References

Abrantes, F., Cermeno, P., Lopes, C., Romero, O., Matos, L., Van Iperen, J., Rufino, M., and Magalhães, V.: Diatoms Si uptake capacity drives carbon export in coastal upwelling systems, Biogeosciences, 13, 4099–4109, https://doi.org/10.5194/bg-13-4099-2016, 2016.

Alfred-Wegener-Institut Helmholtz-Zentrum für Polar- und Meeresforschung: Marine Stations Helgoland and Sylt operated by the Alfred Wegener Institute Helmholtz Centre for Polar and Marine Research, Journal of Large-Scale Research Facilities, 8, A184, https://doi.org/10.17815/jlsrf-8-184, 2023.

Anderson, H. J., Mongin, M., and Matear, R. J.: Ocean alkalinity enhancement in a coastal channel: simulating localised

dispersion, carbon sequestration and ecosystem impact, Environ. Res. Commun., 7, 041012, https://doi.org/10.1088/2515-7620/adce5a, 2025.

Antoni, D., Wichels, A., Boersma, M., and Gerdts, G.: The effect of ocean alkalinity enhancement on pelagic bacterial communities: focus points derived from a mesocosm experiment, Front. Microbiom., 4, 1606890, https://doi.org/10.3389/frmbi.2025.1606890, 2025.

Armstrong, R. A., Lee, C., Hedges, J. I., Honjo, S., and Wakeham, S. G.: A new, mechanistic model for organic carbon fluxes in the ocean based on the quantitative association of POC with ballast minerals, Deep-Sea Res. Pt. II, 49, 219–236, https://doi.org/10.1016/S0967-0645(01)00101-1, 2001.

Azetsu-Scott, K. and Passow, U.: Ascending marine particles: Significance of transparent exopolymer particles (TEP) in the upper ocean, Limnol. Oceanogr., 49, 741–748, https://doi.org/10.4319/lo.2004.49.3.0741, 2004.

Bach, L. T. and Taucher, J.: CO_2 effects on diatoms: a synthesis of more than a decade of ocean acidification experiments with natural communities, Ocean Sci., 15, 1159–1175, https://doi.org/10.5194/os-15-1159-2019, 2019.

Bach, L. T., Riebesell, U., Sett, S., Febiri, S., Rzepka, P., and Schulz, K. G.: An approach for particle sinking velocity measurements in the 3–400 µm size range and considerations on the effect of temperature on sinking rates, Mar. Biol., 159, 1853–1864, https://doi.org/10.1007/s00227-012-1945-2, 2012.

Bach, L. T., Gill, S. J., Rickaby, R. E. M., Gore, S., and Renforth, P.: CO_2 Removal With Enhanced Weathering and Ocean Alkalinity Enhancement: Potential Risks and Co-benefits for Marine Pelagic Ecosystems, Frontiers in Climate, 1, 7, https://doi.org/10.3389/fclim.2019.00007, 2019a.

Bach, L. T., Hernández-Hernández, N., Taucher, J., Spisla, C., Sforna, C., Riebesell, U., and Arístegui, J.: Effects of Elevated CO_2 on a Natural Diatom Community in the Subtropical NE Atlantic, Front. Mar. Sci., 6, 75, https://doi.org/10.3389/fmars.2019.00075, 2019b.

Bach, L. T., Stange, P., Taucher, J., Achterberg, E. P., Algueró-Muñiz, M., Horn, H., Esposito, M., and Riebesell, U.: The Influence of Plankton Community Structure on Sinking Velocity and Remineralization Rate of Marine Aggregates, Global Biogeochem. Cy., 33, 971–994, https://doi.org/10.1029/2019GB006256, 2019c.

Barker, P., Fontes, J., and Gasse, F.: Experimental dissolution of diatom silica in concentrated salt solutions and implications for paleoenvironmental reconstruction, Limnol. Oceanogr., 39, 99–110, https://doi.org/10.4319/lo.1994.39.1.0099, 1994.

Baumann, M., Taucher, J., Paul, A. J., Heinemann, M., Vanharanta, M., Bach, L. T., Spilling, K., Ortiz, J., Arístegui, J., Hernández-Hernández, N., Baños, I., and Riebesell, U.: Effect of Intensity and Mode of Artificial Upwelling on Particle Flux and Carbon Export, Front. Mar. Sci., 8, 742142, https://doi.org/10.3389/fmars.2021.742142, 2021.

Baumann, M., Paul, A. J., Taucher, J., Bach, L. T., Goldenberg, S., Stange, P., Minutolo, F., and Riebesell, U.: Drivers of particle sinking velocities in the Peruvian upwelling system, Biogeosciences, 20, 2595–2612, https://doi.org/10.5194/bg-20-2595-2023, 2023.

Beucher, C., Tréguer, P., Corvaisier, R., Hapette, A., and Elskens, M.: Production and dissolution of biosilica, and changing microphytoplankton dominance in the Bay of Brest (France), Mar. Ecol. Prog. Ser., 267, 57–69, https://doi.org/10.3354/meps267057, 2004.

Bidle, K. D. and Azam, F.: Accelerated dissolution of diatom silica by marine bacterial assemblages, Nature, 397, 508–512, https://doi.org/10.1038/17351, 1999.

Borges, A. V., Delille, B., and Frankignoulle, M.: Budgeting sinks and sources of CO_2 in the coastal ocean: Diversity of ecosystems counts, Geophys. Res. Lett., 32, https://doi.org/10.1029/2005GL023053, 2005.

Boxhammer, T., Bach, L. T., Czerny, J., and Riebesell, U.: Technical note: Sampling and processing of mesocosm sediment trap material for quantitative biogeochemical analysis, Biogeosciences, 13, 2849–2858, https://doi.org/10.5194/bg-13-2849-2016, 2016.

Boyd, P. W. and Newton, P. P.: Does planktonic community structure determine downward particulate organic carbon flux in different oceanic provinces?, Deep Sea Res. Pt. I, 46, 63–91, https://doi.org/10.1016/S0967-0637(98)00066-1, 1999.

Boyd, P. W., Claustre, H., Levy, M., Siegel, D. A., and Weber, T.: Multi-faceted particle pumps drive carbon sequestration in the ocean, Nature, 568, 327–335, https://doi.org/10.1038/s41586-019-1098-2, 2019.

Bradski, G.: The opencv library, https://opencv.org/ (last access: 10 November 2025), 2000.

Brady, P. V. and Walther, J. V.: Controls on silicate dissolution rates in neutral and basic pH solutions at 25° C, Geochim. Cosmochim. Ac., 53, 2823–2830, https://doi.org/10.1016/0016-7037(89)90160-9, 1989.

Bryan, J. R., Rlley, J. P., and Williams, P. J. Leb.: A winkler procedure for making precise measurements of oxygen concentration for productivity and related studies, J. Exp. Mar. Biol. Ecol., 21, 191–197, https://doi.org/10.1016/0022-0981(76)90114-3, 1976.

Brzezinski, M. A., Krause, J. W., Bundy, R. M., Barbeau, K. A., Franks, P., Goericke, R., Landry, M. R., and Stukel, M. R.: Enhanced silica ballasting from iron stress sustains carbon export in a frontal zone within the California Current: Silica ballasting and iron stress, J. Geophys. Res.-Oceans, 120, 4654–4669, https://doi.org/10.1002/2015JC010829, 2015.

Carritt, D. E. and Carpenter, J. H.: Comparison and evaluation of currently employed modifications of the Winkler method for determining dissolved oxygen in seawater; a NASCO report, J. Mar. Res., 24, 286–318, ISSN 0022-2402, 1966.

Caserini, S., Pagano, D., Campo, F., Abbà, A., De Marco, S., Righi, D., Renforth, P., and Grosso, M.: Potential of Maritime Transport for Ocean Liming and Atmospheric CO_2 Removal, Frontiers in Climate, 3, 575900, https://doi.org/10.3389/fclim.2021.575900, 2021.

Clements, D. J., Yang, S., Weber, T., McDonnell, A. M. P., Kiko, R., Stemmann, L., and Bianchi, D.: New Estimate of Organic Carbon Export From Optical Measurements Reveals the Role of Particle Size Distribution and Export Horizon, Global Biogeochem. Cy., 37, https://doi.org/10.1029/2022GB007633, 2023.

Cloern, J. E.: Phytoplankton bloom dynamics in coastal ecosystems: A review with some general lessons from sustained investigation of San Francisco Bay, California, Rev. Geophys., 34, 127–168, https://doi.org/10.1029/96RG00986, 1996.

Coverly, S., Kérouel, R., and Aminot, A.: A re-examination of matrix effects in the segmented-flow analysis of nutrients

in sea and estuarine water, Anal. Chim. Acta, 712, 94–100, https://doi.org/10.1016/j.aca.2011.11.008, 2012.

De Castro, I., Ribeiro, S. C., Louvado, A., Gomes, N. C. M., Cachão, M., Brito De Azevedo, E., and Barcelos E Ramos, J.: Ocean liming effect on a North Atlantic microbial community: changes in composition and rates, Front. Mar. Sci., 12, 1602158, https://doi.org/10.3389/fmars.2025.1602158, 2025.

Dickson, A.: Standards for Ocean Measurements, Oceanography, 23, 34–47, https://doi.org/10.5670/oceanog.2010.22, 2010.

Dickson, A. G., Sabine, C. L., Christian, J. R., Bargeron, C. P., and North Pacific Marine Science Organization: Guide to best practices for ocean CO_2 measurements, edited by: North Pacific Marine Science Organization, Sidney, BC, ISBN 978-1-897176-07-8, 2007.

Doney, S. C., Fabry, V. J., Feely, R. A., and Kleypas, J. A.: Ocean Acidification: The Other CO_2 Problem, Annu. Rev. Mar. Sci., 1, 169–192, https://doi.org/10.1146/annurev.marine.010908.163834, 2009.

Dove, P. M. and Elston, S. F.: Dissolution kinetics of quartz in sodium chloride solutions: Analysis of existing data and a rate model for 25 °C, Geochim. Cosmochim. Ac., 56, 4147–4156, https://doi.org/10.1016/0016-7037(92)90257-J, 1992.

Dupont, S. and Metian, M.: General considerations for experimental research on ocean alkalinity enhancement, State Planet, 1–11, https://doi.org/10.5194/sp-2-oae2023-4-2023, 2023.

Dutkiewicz, S., Morris, J. J., Follows, M. J., Scott, J., Levitan, O., Dyhrman, S. T., and Berman-Frank, I.: Impact of ocean acidification on the structure of future phytoplankton communities, Nat. Clim. Change, 5, 1002–1006, https://doi.org/10.1038/nclimate2722, 2015.

Eisaman, M. D., Geilert, S., Renforth, P., Bastianini, L., Campbell, J., Dale, A. W., Foteinis, S., Grasse, P., Hawrot, O., Löscher, C. R., Rau, G. H., and Rønning, J.: Assessing the technical aspects of ocean-alkalinity-enhancement approaches, State Planet, 1–29, https://doi.org/10.5194/sp-2-oae2023-3-2023, 2023.

Feng, E. Y., Koeve, W., Keller, D. P., and Oschlies, A.: Model-Based Assessment of the CO_2 Sequestration Potential of Coastal Ocean Alkalinization, Earth's Future, 5, 1252–1266, https://doi.org/10.1002/2017EF000659, 2017.

Ferderer, A., Chase, Z., Kennedy, F., Schulz, K. G., and Bach, L. T.: Assessing the influence of ocean alkalinity enhancement on a coastal phytoplankton community, Biogeosciences, 19, 5375–5399, https://doi.org/10.5194/bg-19-5375-2022, 2022.

Ferderer, A., Schulz, K. G., Riebesell, U., Baker, K. G., Chase, Z., and Bach, L. T.: Investigating the effect of silicate- and calcium-based ocean alkalinity enhancement on diatom silicification, Biogeosciences, 21, 2777–2794, https://doi.org/10.5194/bg-21-2777-2024, 2024.

Ferderer, A., Schulz, K. G., Willis, A., Baker, K. G., Chase, Z., and Bach, L. T.: Carbonate chemistry fitness landscapes inform diatom resilience to future perturbations, Sci. Adv., 11, https://doi.org/10.1126/sciadv.adu8024, 2025.

Gao, K. and Campbell, D. A.: Photophysiological responses of marine diatoms to elevated CO_2 and decreased pH: a review, Funct. Plant Biol., 41, 449–459, https://doi.org/10.1071/FP13247, 2014.

Gately, J. A., Kim, S. M., Jin, B., Brzezinski, M. A., and Iglesias-Rodriguez, M. D.: Coccolithophores and diatoms resilient to ocean alkalinity enhancement: A glimpse of hope?, Sci. Adv., 9, https://doi.org/10.1126/sciadv.adg6066, 2023.

Gattuso, J.-P., Magnan, A., Billé, R., Cheung, W. W. L., Howes, E. L., Joos, F., Allemand, D., Bopp, L., Cooley, S. R., Eakin, C. M., Hoegh-Guldberg, O., Kelly, R. P., Pörtner, H.-O., Rogers, A. D., Baxter, J. M., Laffoley, D., Osborn, D., Rankovic, A., Rochette, J., Sumaila, U. R., Treyer, S., and Turley, C.: Contrasting futures for ocean and society from different anthropogenic CO_2 emissions scenarios, Science, 349, https://doi.org/10.1126/science.aac4722, 2015.

Gattuso, J.-P., Magnan, A. K., Bopp, L., Cheung, W. W. L., Duarte, C. M., Hinkel, J., Mcleod, E., Micheli, F., Oschlies, A., Williamson, P., Billé, R., Chalastani, V. I., Gates, R. D., Irisson, J.-O., Middelburg, J. J., Pörtner, H.-O., and Rau, G. H.: Ocean Solutions to Address Climate Change and Its Effects on Marine Ecosystems, Front. Mar. Sci., 5, 337, https://doi.org/10.3389/fmars.2018.00337, 2018.

Gattuso, J.-P., Williamson, P., Duarte, C. M., and Magnan, A. K.: The Potential for Ocean-Based Climate Action: Negative Emissions Technologies and Beyond, Frontiers in Climate, 2, 575716, https://doi.org/10.3389/fclim.2020.575716, 2021.

Grasshoff, K., Kremling, K., and Ehrhardt, M. (Eds.): Methods of Seawater Analysis, 1st ed., Wiley, https://doi.org/10.1002/9783527613984, 1999.

Greenwood, J. E., Truesdale, V. W., and Rendell, A. R.: Toward an Understanding of Biogenic-silica Dissolution in Seawater – An Initial Rate Approach Applied between 40 and 90 ° C, Aquat. Geochem., 11, 1–20, https://doi.org/10.1007/s10498-004-9515-y, 2005.

Groppelli, S., Calvi, D., Comazzi, F., Alamooti, S. J., Azzellino, A., Barbaccia, E., Caronni, S., Macchi, P., Raos, G., and Basso, D.: The response of phytoplankton to pH-equilibrated ocean alkalinization: A mesocosm experiment with harbour waters, Mar. Pollut. Bull., 222, 118787, https://doi.org/10.1016/j.marpolbul.2025.118787, 2026.

Grossart, H.-P. and Ploug, H.: Microbial degradation of organic carbon and nitrogen on diatom aggregates, Limnol. Oceanogr., 46, 267–277, https://doi.org/10.4319/lo.2001.46.2.0267, 2001.

Guidi, L., Stemmann, L., Jackson, G. A., Ibanez, F., Claustre, H., Legendre, L., Picheral, M., and Gorskya, G.: Effects of phytoplankton community on production, size, and export of large aggregates: A world-ocean analysis, Limnol. Oceanogr., 54, 1951–1963, https://doi.org/10.4319/lo.2009.54.6.1951, 2009.

Guo, J. A., Strzepek, R. F., Swadling, K. M., Townsend, A. T., and Bach, L. T.: Influence of ocean alkalinity enhancement with olivine or steel slag on a coastal plankton community in Tasmania, Biogeosciences, 21, 2335–2354, https://doi.org/10.5194/bg-21-2335-2024, 2024.

Guo, J. A., Strzepek, R. F., Yuan, Z., Swadling, K. M., Townsend, A. T., Achterberg, E. P., Browning, T. J., and Bach, L. T.: Effects of ocean alkalinity enhancement on plankton in the Equatorial Pacific, Communications Earth & Environment, 6, 270, https://doi.org/10.1038/s43247-025-02248-7, 2025.

Hansen, H. P. and Koroleff, F.: Determination of nutrients, in: Methods of Seawater Analysis, edited by: Grasshoff, K., Kremling, K., and Ehrhardt, M., Wiley, 159–228, https://doi.org/10.1002/9783527613984.ch10, 1999.

Hansen, P.: Effect of high pH on the growth and survival of marine phytoplankton: implications for species succession, Aquat.

Microb. Ecol., 28, 279–288, https://doi.org/10.3354/ame028279, 2002.

Hartmann, J., Suitner, N., Lim, C., Schneider, J., Marín-Samper, L., Arístegui, J., Renforth, P., Taucher, J., and Riebesell, U.: Stability of alkalinity in ocean alkalinity enhancement (OAE) approaches – consequences for durability of CO_2 storage, Biogeosciences, 20, 781–802, https://doi.org/10.5194/bg-20-781-2023, 2023.

Hashim, M. S., Marx, L., Klein, F., Dean, C. L., Burdige, E., Hayden, M., McCorkle, D. C., and Subhas, A. V.: Mineral formation during shipboard ocean alkalinity enhancement experiments in the North Atlantic, Biogeosciences, 22, 7149–7165, https://doi.org/10.5194/bg-22-7149-2025, 2025.

He, J. and Tyka, M. D.: Limits and CO_2 equilibration of near-coast alkalinity enhancement, Biogeosciences, 20, 27–43, https://doi.org/10.5194/bg-20-27-2023, 2023.

Hervé, V., Derr, J., Douady, S., Quinet, M., Moisan, L., and Lopez, P. J.: Multiparametric Analyses Reveal the pH-Dependence of Silicon Biomineralization in Diatoms, PLoS ONE, 7, https://doi.org/10.1371/journal.pone.0046722, 2012.

Honjo, S., Manganini, S. J., Krishfield, R. A., and Francois, R.: Particulate organic carbon fluxes to the ocean interior and factors controlling the biological pump: A synthesis of global sediment trap programs since 1983, Prog. Oceanogr., 76, 217–285, https://doi.org/10.1016/j.pocean.2007.11.003, 2008.

Iglesias-Rodríguez, M. D., Rickaby, R. E. M., Singh, A., and Gately, J. A.: Laboratory experiments in ocean alkalinity enhancement research, State Planet, 1–18, https://doi.org/10.5194/sp-2-oae2023-5-2023, 2023.

Jones, D. C., Ito, T., Takano, Y., and Hsu, W.: Spatial and seasonal variability of the air-sea equilibration timescale of carbon dioxide, Global Biogeochem. Cy., 28, 1163–1178, https://doi.org/10.1002/2014GB004813, 2014.

Karakuş, O., Nissen, C., Völker, C., Hagen, W., Iversen, M., Oziel, L., Gürses, Ö., and Hauck, J.: The Role of Ballasting, Seawater Viscosity and Oxygen-Dependent Remineralization for Export and Transfer Efficiencies in the Global Ocean, Global Biogeochem. Cy., 39, https://doi.org/10.1029/2024GB008403, 2025.

Kauppi, L., Norkko, J., Ikonen, J., and Norkko, A.: Seasonal variability in ecosystem functions: quantifying the contribution of invasive species to nutrient cycling in coastal ecosystems, Mar. Ecol. Prog. Ser., 572, 193–207, https://doi.org/10.3354/meps12171, 2017.

Kirchner, J. S., Lettmann, K. A., Schnetger, B., Wolff, J.-O., and Brumsack, H.-J.: Carbon capture via accelerated weathering of limestone: Modeling local impacts on the carbonate chemistry of the southern North Sea, Int. J. Greenh. Gas Con., 92, 102855, https://doi.org/10.1016/j.ijggc.2019.102855, 2020.

Köhler, P., Hartmann, J., and Wolf-Gladrow, D. A.: Geoengineering potential of artificially enhanced silicate weathering of olivine, P. Natl. Acad. Sc., 107, 20228–20233, https://doi.org/10.1073/pnas.1000545107, 2010.

Kousoulas, K., Ferderer, A., Eriksen, R., and Bach, L. T.: Winners and losers under hydroxide-based ocean alkalinity enhancement in a Tasmanian plankton community, J. Phycol., 61, 989–1006, https://doi.org/10.1111/jpy.70052, 2025.

Laurenceau-Cornec, E. C., Le Moigne, F. A. C., Gallinari, M., Moriceau, B., Toullec, J., Iversen, M. H., Engel, A., and De La Rocha, C. L.: New guidelines for the application of Stokes' models to the sinking velocity of marine aggregates, Limnol. Oceanogr., 65, 1264–1285, https://doi.org/10.1002/lno.11388, 2020.

Le Moigne, F. A. C., Sanders, R. J., Villa-Alfageme, M., Martin, A. P., Pabortsava, K., Planquette, H., Morris, P. J., and Thomalla, S. J.: On the proportion of ballast versus non-ballast associated carbon export in the surface ocean, Geophys. Res. Lett., 39, https://doi.org/10.1029/2012GL052980, 2012.

Le Moigne, F. A. C., Henson, S. A., Cavan, E., Georges, C., Pabortsava, K., Achterberg, E. P., Ceballos-Romero, E., Zubkov, M., and Sanders, R. J.: What causes the inverse relationship between primary production and export efficiency in the Southern Ocean?, Geophys. Res. Lett., 43, 4457–4466, https://doi.org/10.1002/2016GL068480, 2016.

Lee, K., Kim, T.-W., Byrne, R. H., Millero, F. J., Feely, R. A., and Liu, Y.-M.: The universal ratio of boron to chlorinity for the North Pacific and North Atlantic oceans, Geochim. Cosmochim. Ac., 74, 1801–1811, https://doi.org/10.1016/j.gca.2009.12.027, 2010.

Lewin, J. C.: The dissolution of silica from diatom walls, Geochim. Cosmochim. Ac., 21, 182–198, https://doi.org/10.1016/S0016-7037(61)80054-9, 1961.

Li, C., Liu, X., Li, Y., Jiang, Y., Guo, X., Hutchins, D. A., Ma, J., Lin, X., and Dai, M.: The interactions between olivine dissolution and phytoplankton in seawater: Potential implications for ocean alkalinization, Sci. Total Environ., 912, 168571, https://doi.org/10.1016/j.scitotenv.2023.168571, 2024.

Malviya, S., Scalco, E., Audic, S., Vincent, F., Veluchamy, A., Poulain, J., Wincker, P., Iudicone, D., De Vargas, C., Bittner, L., Zingone, A., and Bowler, C.: Insights into global diatom distribution and diversity in the world's ocean, P. Natl. Ac. Sci., 113, https://doi.org/10.1073/pnas.1509523113, 2016.

Marie, D., Partensky, F., Vaulot, D., and Brussaard, C.: Enumeration of Phytoplankton, Bacteria, and Viruses in Marine Samples, CP Cytometry, 10, https://doi.org/10.1002/0471142956.cy1111s10, 1999.

Marín-Samper, L., Arístegui, J., Hernández-Hernández, N., Ortiz, J., Archer, S. D., Ludwig, A., and Riebesell, U.: Assessing the impact of CO_2-equilibrated ocean alkalinity enhancement on microbial metabolic rates in an oligotrophic system, Biogeosciences, 21, 2859–2876, https://doi.org/10.5194/bg-21-2859-2024, 2024.

Marín-Samper, L., Arístegui, J., Hernández-Hernández, N., and Riebesell, U.: Responses of microbial metabolic rates to non-equilibrated silicate- versus calcium-based ocean alkalinity enhancement, Biogeosciences, 21, 5707–5724, https://doi.org/10.5194/bg-21-5707-2024, 2024b.

Martin-Jézéquel, V., Hildebrand, M., and Brzezinski, M. A.: Silicon metabolism in diatoms: implications for growth, J. Phycol., 36, 821–840, https://doi.org/10.1046/j.1529-8817.2000.00019.x, 2000.

Mathis, M., Lacroix, F., Hagemann, S., Nielsen, D. M., Ilyina, T., and Schrum, C.: Enhanced CO_2 uptake of the coastal ocean is dominated by biological carbon fixation, Nat. Clim. Change, 14, 373–379, https://doi.org/10.1038/s41558-024-01956-w, 2024.

Moras, C. A., Bach, L. T., Cyronak, T., Joannes-Boyau, R., and Schulz, K. G.: Ocean alkalinity enhancement – avoiding runaway $CaCO_3$ precipitation during quick and hydrated lime dissolution,

Biogeosciences, 19, 3537–3557, https://doi.org/10.5194/bg-19-3537-2022, 2022.

Moriceau, B., Garvey, M., Ragueneau, O., and Passow, U.: Evidence for reduced biogenic silica dissolution rates in diatom aggregates, Mar. Ecol. Prog. Ser., 333, 129–142, https://doi.org/10.3354/meps333129, 2007.

Moriceau, B., Laruelle, G., Passow, U., Van Cappellen, P., and Ragueneau, O.: Biogenic silica dissolution in diatom aggregates: insights from reactive transport modelling, Mar. Ecol. Prog. Ser., 517, 35–49, https://doi.org/10.3354/meps11028, 2014.

Oberlander, J. L., Burke, M. E., London, C. A., and MacIntyre, H. L.: Assessing the impacts of simulated ocean alkalinity enhancement on viability and growth of nearshore species of phytoplankton, Biogeosciences, 22, 499–512, https://doi.org/10.5194/bg-22-499-2025, 2025.

Passow, U., Engel, A., and Ploug, H.: The role of aggregation for the dissolution of diatom frustules, FEMS Microbiol. Ecol., 46, 247–255, https://doi.org/10.1016/S0168-6496(03)00199-5, 2003.

Paul, A. J., Haunost, M., Goldenberg, S. U., Hartmann, J., Sánchez, N., Schneider, J., Suitner, N., and Riebesell, U.: Ocean alkalinity enhancement in an open-ocean ecosystem: biogeochemical responses and carbon storage durability, Biogeosciences, 22, 2749–2766, https://doi.org/10.5194/bg-22-2749-2025, 2025.

Perez, F. F. and Fraga, F.: Association constant of fluoride and hydrogen ions in seawater, Mar. Chem., 21, 161–168, https://doi.org/10.1016/0304-4203(87)90036-3, 1987.

Petrou, K., Baker, K. G., Nielsen, D. A., Hancock, A. M., Schulz, K. G., and Davidson, A. T.: Acidification diminishes diatom silica production in the Southern Ocean, Nat. Clim. Change, 9, 781–786, https://doi.org/10.1038/s41558-019-0557-y, 2019.

Pierella Karlusich, J. J., Bowler, C., and Biswas, H.: Carbon Dioxide Concentration Mechanisms in Natural Populations of Marine Diatoms: Insights From Tara Oceans, Front. Plant Sci., 12, 657821, https://doi.org/10.3389/fpls.2021.657821, 2021.

Pierrot, D., Epitalon, J.-M., Orr, J. C., Lewis, E., and Wallace, D. W. R.: MS Excel program developed for CO_2 system calculations – version 3.0, GitHub [code], https://github.com/dpierrot/co2sys_xl (last access: 15 October 2025), 2021.

Ploug, H., Hietanen, S., and Kuparinen, J.: Diffusion and advection within and around sinking, porous diatom aggregates, Limnol. Oceanogr., 47, 1129–1136, https://doi.org/10.4319/lo.2002.47.4.1129, 2002.

Puigcorbé, V., Benitez-Nelson, C. R., Masqué, P., Verdeny, E., White, A. E., Popp, B. N., Prahl, F. G., and Lam, P. J.: Small phytoplankton drive high summertime carbon and nutrient export in the Gulf of California and Eastern Tropical North Pacific, Global Biogeochem. Cy., 29, 1309–1332, https://doi.org/10.1002/2015GB005134, 2015.

R Core Team: R: A Language and Environment for Statistical Computing, R Foundation for Statistical Computing, Vienna, Austria, https://www.R-project.org/ (last access: 12 December 2025), 2021.

Ragueneau, O., Schultes, S., Bidle, K., Claquin, P., and Moriceau, B.: Si and C interactions in the world ocean: Importance of ecological processes and implications for the role of diatoms in the biological pump, Global Biogeochem. Cy., 20, https://doi.org/10.1029/2006GB002688, 2006.

Raven, J. A.: Limits on growth rates, Nature, 361, 209–210, https://doi.org/10.1038/361209a0, 1993.

Renforth, P. and Henderson, G.: Assessing ocean alkalinity for carbon sequestration, Rev. Geophys., 55, 636–674, https://doi.org/10.1002/2016RG000533, 2017.

Riebesell, U., Wolf-Gladrow, D. A., and Smetacek, V.: Carbon dioxide limitation of marine phytoplankton growth rates, Nature, 361, 249–251, https://doi.org/10.1038/361249a0, 1993.

Riebesell, U., Czerny, J., von Bröckel, K., Boxhammer, T., Büdenbender, J., Deckelnick, M., Fischer, M., Hoffmann, D., Krug, S. A., Lentz, U., Ludwig, A., Muche, R., and Schulz, K. G.: Technical Note: A mobile sea-going mesocosm system – new opportunities for ocean change research, Biogeosciences, 10, 1835–1847, https://doi.org/10.5194/bg-10-1835-2013, 2013.

Riebesell, U., Basso, D., Geilert, S., Dale, A. W., and Kreuzburg, M.: Mesocosm experiments in ocean alkalinity enhancement research, State Planet, 1–14, https://doi.org/10.5194/sp-2-oae2023-6-2023, 2023.

Ristow, G. H.: Wall correction factor for sinking cylinders in fluids, Phys. Rev., 55, 2808–2813, https://doi.org/10.1103/PhysRevE.55.2808, 1997.

Rogelj, J., Popp, A., Calvin, K. V., Luderer, G., Emmerling, J., Gernaat, D., Fujimori, S., Strefler, J., Hasegawa, T., Marangoni, G., Krey, V., Kriegler, E., Riahi, K., Van Vuuren, D. P., Doelman, J., Drouet, L., Edmonds, J., Fricko, O., Harmsen, M., Havlík, P., Humpenöder, F., Stehfest, E., and Tavoni, M.: Scenarios towards limiting global mean temperature increase below 1.5 ° C, Nature Clim. Change, 8, 325–332, https://doi.org/10.1038/s41558-018-0091-3, 2018.

Rost, B., Zondervan, I., and Wolf-Gladrow, D.: Sensitivity of phytoplankton to future changes in ocean carbonate chemistry: current knowledge, contradictions and research directions, Mar. Ecol. Prog. Ser., 373, 227–237, https://doi.org/10.3354/meps07776, 2008.

Roy, S. (Ed.): Phytoplankton pigments: characterization, chemotaxonomy, and applications in oceanography, Cambridge University Press, Cambridge; New York, 845 pp., ISBN: 978-1-107-00066-7, 2011.

Sánchez, N., Goldenberg, S. U., Brüggemann, D., Jaspers, C., Taucher, J., and Riebesell, U.: Plankton food web structure and productivity under ocean alkalinity enhancement, Sci. Adv., 10, https://doi.org/10.1126/sciadv.ado0264, 2024.

Sarmiento, J. L.: Ocean biogeochemical dynamics, Princeton University Press, ISBN 1-4008-4907-1, 2006.

Sarthou, G., Timmermans, K. R., Blain, S., and Tréguer, P.: Growth physiology and fate of diatoms in the ocean: a review, J. Sea Res., 53, 25–42, https://doi.org/10.1016/j.seares.2004.01.007, 2005.

Schneider, J., Riebesell, U., Moras, C. A., Marín-Samper, L., Kittu, L. R., Ortíz-Cortes, J., and Schulz, K. G.: Carbon fixation of a temperate plankton community in response to calcium- and silicate-based Ocean Alkalinity Enhancement using air-sea gas exchange measurements, Biogeosciences, 23, 137–153, https://doi.org/10.5194/bg-23-137-2026, 2026.

Schulz, K. G., Bach, L. T., and Dickson, A. G.: Seawater carbonate chemistry considerations for ocean alkalinity enhancement research: theory, measurements, and calculations, State Planet, 1–14, https://doi.org/10.5194/sp-2-oae2023-2-2023, 2023.

Schulz, K. G., Schneider, J., and Riebesell, U.: Carbonate chemistry speciation of the 2023 KOSMOS Helgoland experiment on the effects of ocean alkalinity enhancement on pelagic foodwebs,

pangaea [data set], https://doi.org/10.1594/PANGAEA.986507, 2025.

Sharp, J. H.: Improved analysis for "particulate" organic carbon and nitrogen from seawater1, Limnol. Oceanogr., 19, 984–989, https://doi.org/10.4319/lo.1974.19.6.0984, 1974.

Siegel, D. A., Buesseler, K. O., Doney, S. C., Sailley, S. F., Behrenfeld, M. J., and Boyd, P. W.: Global assessment of ocean carbon export by combining satellite observations and food-web models, Global Biogeochem. Cy., 28, 181–196, https://doi.org/10.1002/2013GB004743, 2014.

Socratis, L., Cappelle, P. V., and Behrends, T.: Dissolution of biogenic silica from land to ocean: Role of salinity and pH, Limnol. Oceanogr., 53, 1614–1621, https://doi.org/10.4319/lo.2008.53.4.1614, 2008.

Sommer, U., Paul, C., and Moustaka-Gouni, M.: Warming and Ocean Acidification Effects on Phytoplankton – From Species Shifts to Size Shifts within Species in a Mesocosm Experiment, PLoS ONE, 10, https://doi.org/10.1371/journal.pone.0125239, 2015.

Stukel, M. R., Landry, M. R., Benitez-Nelson, C. R., and Goericke, R.: Trophic cycling and carbon export relationships in the California Current Ecosystem, Limnol. Oceanogr., 56, 1866–1878, https://doi.org/10.4319/lo.2011.56.5.1866, 2011.

Stukel, M. R., Irving, J. P., Kelly, T. B., Ohman, M. D., Fender, C. K., and Yingling, N.: Carbon sequestration by multiple biological pump pathways in a coastal upwelling biome, Nature Communications, 14, 2024, https://doi.org/10.1038/s41467-023-37771-8, 2023.

Subhas, A. V., Marx, L., Reynolds, S., Flohr, A., Mawji, E. W., Brown, P. J., and Cael, B. B.: Microbial ecosystem responses to alkalinity enhancement in the North Atlantic Subtropical Gyre, Frontiers in Climate, 4, 784997, https://doi.org/10.3389/fclim.2022.784997, 2022.

Suessle, P., Taucher, J., Goldenberg, S. U., Baumann, M., Spilling, K., Noche-Ferreira, A., Vanharanta, M., and Riebesell, U.: Particle fluxes by subtropical pelagic communities under ocean alkalinity enhancement, Biogeosciences, 22, 71–86, https://doi.org/10.5194/bg-22-71-2025, 2025.

Suessle, P., Schulz, K. G., Barcelos E Ramos, J., Sievers, N. M., and Riebesell, U.: KOSMOS 2023 Helgoland mesocosm study on ocean alkalinity enhancement: sediment trap particle flux data and water column biogeochemistry, PANGAEA [data set], https://doi.org/10.1594/PANGAEA.992023, 2026.

Sulpis, O., Lauvset, S. K., and Hagens, M.: Current estimates of K_1 and K_2 appear inconsistent with measured CO_2 system parameters in cold oceanic regions, Ocean Sci., 16, 847–862, https://doi.org/10.5194/os-16-847-2020, 2020.

Tammen, J. K., Kittu, L., Schartau, M., Faucher, G., Schulz, K. G., and Riebesell, U.: KOSMOS 2023 Helgoland mesocosm study on ocean alkalinity enhancement: dissolved inorganic nutrients, chlorophyll a and suspended particulate organic matter, PANGAEA [data set], https://doi.pangaea.de/10.1594/PANGAEA.987501, 2026.

Taucher, J., Bach, L. T., Prowe, A. E. F., Boxhammer, T., Kvale, K., and Riebesell, U.: Enhanced silica export in a future ocean triggers global diatom decline, Nature, 605, 696–700, https://doi.org/10.1038/s41586-022-04687-0, 2022.

Timmermans, K. R., Van Der Wagt, B., and De Baar, H. J. W.: Growth rates, half-saturation constants, and silicate, nitrate, and phosphate depletion in relation to iron availability of four large, open-ocean diatoms from the Southern Ocean, Limnol. Oceanogr., 49, 2141–2151, https://doi.org/10.4319/lo.2004.49.6.2141, 2004.

Tréguer, P., Bowler, C., Moriceau, B., Dutkiewicz, S., Gehlen, M., Aumont, O., Bittner, L., Dugdale, R., Finkel, Z., Iudicone, D., Jahn, O., Guidi, L., Lasbleiz, M., Leblanc, K., Levy, M., and Pondaven, P.: Influence of diatom diversity on the ocean biological carbon pump, Nature Geosci., 11, 27–37, https://doi.org/10.1038/s41561-017-0028-x, 2018.

Van Cappellen, P., Dixit, S., and Van Beusekom, J.: Biogenic silica dissolution in the oceans: Reconciling experimental and field-based dissolution rates, Global Biogeochem. Cy., 16, https://doi.org/10.1029/2001GB001431, 2002.

Van Heukelem, L. and Thomas, C. S.: Computer-assisted high-performance liquid chromatography method development with applications to the isolation and analysis of phytoplankton pigments, J. Chromatogr. A, 910, 31–49, https://doi.org/10.1016/S0378-4347(00)00603-4, 2001.

Van Rossum, G.: Python programming language, http://www.python.org (last access: 10 November 2025), 2007.

Vrieling, E. G., Gieskes, W. W. C., and Beelen, T. P. M.: Silicon deposition in diatoms: control by the pH inside the deposition vesicle, J. Phycol., 35, 548–559, https://doi.org/10.1046/j.1529-8817.1999.3530548.x, 1999.

Wickham, H.: ggplot2: Elegant Graphics for Data Analysis, Springer-Verlag New York, https://ggplot2.tidyverse.org (last access: 20 December 2025), 2016.

Wiltshire, K. H., Kraberg, A., Bartsch, I., Boersma, M., Franke, H.-D., Freund, J., Gebühr, C., Gerdts, G., Stockmann, K., and Wichels, A.: Helgoland Roads, North Sea: 45 Years of Change, Estuar. Coasts, 33, 295–310, https://doi.org/10.1007/s12237-009-9228-y, 2010.

Wu, Y., Campbell, D. A., Irwin, A. J., Suggett, D. J., and Finkel, Z. V.: Ocean acidification enhances the growth rate of larger diatoms, Limnol. Oceanogr., 59, 1027–1034, https://doi.org/10.4319/lo.2014.59.3.1027, 2014.

Xin, X., Goldenberg, S. U., Taucher, J., Stuhr, A., Arístegui, J., and Riebesell, U.: Resilience of Phytoplankton and Microzooplankton Communities under Ocean Alkalinity Enhancement in the Oligotrophic Ocean, Environ. Sci. Technol., 58, 20918–20930, https://doi.org/10.1021/acs.est.4c09838, 2024.

Zeebe, R. and Wolf-Gladrow, D.: CO_2 in seawater: equilibrium, kinetics, isotopes, Transferred to digital printing., Elsevier, Amsterdam, ISBN 978-0-444-50946-8, 2007.

Zeileis, A. and Grothendieck, G.: zoo: S3 Infrastructure for Regular and Irregular Time Series, J. Stat. Softw., 14, https://cran.r-project.org/web/packages/zoo/ (last access: 12 December 2025), 2005.

Zeileis, A. and Hothorn, T.: Diagnostic Checking in Regression Relationships, R News, 2, 7–10, https://CRAN.R-project.org/package=lmtest (last access: 12 December 2025), 2002.

Zhou, M., Tyka, M. D., Ho, D. T., Yankovsky, E., Bachman, S., Nicholas, T., Karspeck, A. R., and Long, M. C.: Mapping the global variation in the efficiency of ocean alkalinity enhancement for carbon dioxide removal, Nat. Clim. Chang., 15, 59–65, https://doi.org/10.1038/s41558-024-02179-9, 2025.